Brain, Behavior, and Immunity xxx (2016) xxx–xxx

Contents lists available at ScienceDirect

Brain, Behavior, and Immunity

journal homepage: www.elsevier.com/locate/ybrbi

The placental interleukin-6 signaling controls fetal brain development and behavior

Wei-Li Wu [a,*], Elaine Y. Hsiao [a,b], Zihao Yan [a], Sarkis K. Mazmanian [a], Paul H. Patterson [a,1]

[a] Division of Biology and Biological Engineering, California Institute of Technology, 1200 E. California Boulevard, Pasadena, CA 91125, USA
[b] Department of Integrative Biology & Physiology, University of California, Los Angeles, 610 Charles E. Young Drive, Los Angeles, CA 90095, USA

ARTICLE INFO

Article history:
Received 27 July 2016
Received in revised form 20 October 2016
Accepted 8 November 2016
Available online xxxx

Keywords:
Maternal immune activation (MIA)
Maternal-placental-fetal axis
Interleukin-6 (IL-6)
Placenta
Hindbrain development
Purkinje cells
Autism spectrum disorder (ASD)

ABSTRACT

Epidemiological studies show that maternal immune activation (MIA) during pregnancy is a risk factor for autism. However, mechanisms for how MIA affects brain development and behaviors in offspring remain poorly described. To determine whether placental interleukin-6 (IL-6) signaling is required for mediating MIA on the offspring, we generated mice with restricted deletion of the receptor for IL-6 (IL-6Rα) in placental trophoblasts (*Cyp19-Cre*$^{+}$;*Il6ra*$^{fl/fl}$), and tested offspring of *Cyp19-Cre*$^{+}$;*Il6ra*$^{fl/fl}$ mothers for immunological, pathological and behavioral abnormalities following induction of MIA. We reveal that MIA results in acute inflammatory responses in the fetal brain. Lack of IL-6 signaling in trophoblasts effectively blocks MIA-induced inflammatory responses in the placenta and the fetal brain. Furthermore, behavioral abnormalities and cerebellar neuropathologies observed in MIA control offspring are prevented in *Cyp19-Cre*$^{+}$;*Il6ra*$^{fl/fl}$ offspring. Our results demonstrate that IL-6 activation in placenta is required for relaying inflammatory signals to the fetal brain and impacting behaviors and neuropathologies relevant to neurodevelopmental disease.

1. Introduction

Autism spectrum disorder (ASD) is a range of complex neurodevelopmental disorders, characterized by difficulties in social communication, and repetitive and stereotyped behaviors (Association, 2013). To date, the prevalence for ASD in the United States is one in 68 children (Investigators, 2014) and diagnoses worldwide are 62 per 10,000 people (Elsabbagh et al., 2012). Monozygotic twins studies indicate the concordance rate for ASD ranges between 60 and 91% (Ronald and Hoekstra, 2011), which suggests both genetic and non-genetic factors (e.g. environment) could contribute to the etiology of ASD.

Epidemiological studies suggest that maternal infection is a principal non-genetic risk factor for ASD (Brown, 2012). Analyses of large cohorts of ASD patients found that inpatient diagnosis of severe infection during pregnancy are associated with increased ASD risk (Atladottir et al., 2010; Lee et al., 2014). The diversity of infections and the observation that many are not transmitted to the fetus (Fatemi et al., 2012; Shi et al., 2005) suggest that maternal immune activation (MIA), rather than microbial pathogenesis, is responsible for increasing the risk of ASD in the offspring. This emphasis on MIA rather than a specific pathogen is supported by animal models that involve injection of non-pathogenic antigens, such as polyinosinic-polycytidylic acid (poly(I:C)) (Boksa, 2010; Meyer, 2014). Stimulation of the maternal immune system in these cases causes offspring to develop behavioral and neuropathological features of ASD similar to those seen in maternal infection (Boksa, 2010; Knuesel et al., 2014; Meyer, 2014).

The molecular mechanisms underlying abnormal neurodevelopment and behavior in MIA are poorly understood, though cytokines appear to be critical (Boksa, 2010; Knuesel et al., 2014). The immune dysregulation in MIA offspring persists postnatally (Garay et al., 2013; Hsiao et al., 2012). MIA causes long-lasting and region specific changes of brain cytokines in the offspring that vary based on developmental time point (Garay et al., 2013). Furthermore, MIA leads to decreases in splenic and mesenteric regulatory T cells (Tregs) and increases in interleukin (IL)-6 and IL-17 production in splenic CD4^{+} T cells in adult offspring (Hsiao et al., 2012). IL-6 levels are elevated in fetal brain after MIA induction (Connor et al., 2012; Meyer et al., 2006; Wu et al., 2015). Blocking IL-6, but not IL-1β or interferon gamma (IFNγ), after induction of MIA in pregnant mice prevents behavioral abnormalities in the offspring (Smith et al., 2007). Furthermore, injection of recombinant

* Corresponding author.
E-mail addresses: wlwu@caltech.edu (W.-L. Wu), ehsiao@ucla.edu (E.Y. Hsiao), Zihao_Yan@hms.harvard.edu (Z. Yan), sarkis@caltech.edu (S.K. Mazmanian), php@caltech.edu (P.H. Patterson).

[1] This study is dedicated to Dr. Paul H. Patterson, who conceived and led the project prior to his passing in 2014.

http://dx.doi.org/10.1016/j.bbi.2016.11.007
0889-1591/

IL-6 alone into mice is sufficient to promote similar behavioral phenotypes seen in the MIA model (Hsiao and Patterson, 2011), arguing for a causal role for IL-6 signaling in this context. The importance of IL-6 in mediating MIA effects on brain and behavior in rodents is also supported by the studies shown in human ASD subjects, wherein IL-6 is increased in ASD subjects (Ashwood et al., 2011; Li et al., 2009; Masi et al., 2014; Vargas et al., 2005; Wei et al., 2011). IL-6 is both necessary and sufficient for mediating the effects of MIA on the development of ASD-related behavioral abnormalities, suggesting that tracing the pathways of MIA-induced IL-6 signaling may reveal novel mechanisms by which maternal insults disrupt fetal neurodevelopment.

The significance of the placenta in the occurrence of psychiatric disorders has been suggested by several studies. The concordance rate of monochorionic twins for schizophrenia is 60%, while dichorionic twins is only 10.7% (Davis et al., 1995). Examining the histology of the placenta from individuals with ASD reveals that about 3–8-fold increased odds of having trophoblast inclusion in the ASD groups compared to controls (Anderson et al., 2007; Walker et al., 2013). These correlations indicate that the uterine environment should also be considered when evaluating potential etiologies for psychiatric disorders.

During infection, increased cytokine levels in the maternal environment might directly transmit signals to the fetus through the placenta (Dahlgren et al., 2006; Zaretsky et al., 2004). Placenta is of fetal origin, juxtaposed against the maternal decidua (D) layer, and represents the primary molecular connection between the mother and its developing fetus. IL-6 production signaling in the placenta, particularly in the spongiotrophoblast (SP) layer, following induction of MIA has been reported (Hsiao and Patterson, 2011). Furthermore, the MIA-induced alterations in IL-6 signaling pathways in the placenta, and placental hormone production following MIA are prevented upon immune-activation of *Il6*$^{-/-}$ pregnant mice (Hsiao and Patterson, 2011), revealing dependence on placental IL-6. Whether placental IL-6 signaling is involved in relaying the detrimental effects of MIA to the developing embryo is unknown.

To understand whether IL-6 signaling in the placenta plays a role in modulating the MIA response, we crossed placental trophoblast specific Cre mice (*Cyp19-Cre*) (Wenzel and Leone, 2007) with IL-6Rα loxp-flanked mice (*Il6ra*$^{fl/fl}$) (McFarland-Mancini et al., 2010) to generate trophoblast-specific IL-6Rα knockout mice (*Cyp19-Cre*$^{+}$;*Il6ra*$^{fl/fl}$). The *Cyp19* gene encodes aromatase cytochrome P450 converting androgens to estrogens, which plays an important role in uterine and placental growth and differentiation (Furbass et al., 2008). Different promoter regions of the *Cyp19* gene drive its expression into different tissues (Rawn and Cross, 2008). The *Cyp19-Cre* 5912 founder line specifically expresses Cre recombinase at placental trophoblast precursor cells during the early stage of embryogenesis and shows minimal expression of Cre recombinase in fetal tissues (Wenzel and Leone, 2007), which allows us to examine the functionality of IL-6 in MIA model specifically in placental trophoblast population. Herein, we reveal that immune activation in the placenta perturbs fetal brain development during gestation, resulting in ASD-like behavioral symptoms in offspring. These findings support a growing appreciation of environmental risk factors for mental disorders.

2. Materials and methods

2.1. Mice

Wild-type C57BL/6N mice were obtained through Caltech's barrier animal facility (originally from Charles River, Wilmington, MA, USA). *Il6*$^{-/-}$ (002650; B6.129S2-*Il6tm1Kopf*/J) and *Il6ra*$^{fl/fl}$ (012944; B6;SJL-*Il6ratm1.1Drew*/J012944) mouse lines were obtained from Jackson Laboratory (Bar Harbor, ME, USA). *Cyp19-Cre* mouse (5912 line) was obtained by Dr. Gustavo Leone from Ohio State University (Wenzel and Leone, 2007). *ROSA::LSL-lacZ* mouse was kindly provided by Dr. David J. Anderson at Caltech. *Ate1*$^{-/-}$ mice were kindly provided by Dr. Alexander J. Varshavsky at Caltech (Brower and Varshavsky, 2009). Mice were maintained at Caltech's barrier animal facility and transferred to Caltech's Broad animal facility for experiments. All mice were group housed (2–5 mice per cage) with a 13 h light/11 h dark cycle (lights on at 06:00) at 21–23 °C and 45% relative humidity within a range of 30–70% in ventilated cages (Super Mouse 750™, Lab Products Inc, Seaford, DE, USA). Pregnant and lactating mice were fed a mix of half 5053 PicoLab Rodent Diet and half 5058 PicoLab Rodent Diet (5053, Lad Diet, St. Louis, MO, USA). All experiments were performed under the approval of the California Institute of Technology Institutional Animal Care and Use Committee (IACUC).

2.2. Generation and genotyping of placental trophoblast IL-6Rα knockout mice

Placental trophoblast IL-6Rα knockout mice, *Cyp19-Cre*$^{+}$; *Il6ra*$^{fl/fl}$, were generated by crossing two mouse lines- *Il6ra*$^{fl/fl}$ and *Cyp19-Cre* (5912 line). To yield a congenic strain of *Cyp19-Cre*$^{+}$; *Il6ra*$^{fl/fl}$ mice, the *Cyp19-Cre*$^{+}$ mouse line was backcrossed to C57BL/6N for at least 8 generations. After backcrossing, C57BL/6N *Cyp19-Cre*$^{+}$ mice were crossed with *Il6ra*$^{fl/fl}$ mice, which were originally derived and maintained on C57BL/6J background. F1 offspring were *Il6ra*$^{fl/+}$ and *Cyp19-Cre*$^{+}$;*Il6ra*$^{fl/+}$. These were then crossed to yield F2: *Il6ra*$^{+/+}$, *Il6ra*$^{fl/+}$, *Il6ra*$^{fl/fl}$, *Cyp19-Cre*$^{+}$; *Il6ra*$^{+/+}$, *Cyp19-Cre*$^{+}$; *Il6ra*$^{fl/+}$, and *Cyp19-Cre*$^{+}$; *Il6ra*$^{fl/fl}$. Offspring of *Il6ra*$^{fl/fl}$ and *Cyp19-Cre*$^{+}$; *Il6ra*$^{fl/fl}$ genotypes were maintained for experiments.

Mice were weaned at the age of 3 weeks. Then the mice were labeled by ear punch and tail snips were collected immediately after weaning. gDNA was extracted using a standard DNA extraction protocol. PCR was performed to amplify a fragment of *Il6* flox allele or wild-type allele. Cre was detected in a separate round of PCR. Primer sequences are listed below.

Il6ra flox allele: Forward 5′-GAA GGA GGA GCT TGA CCT TGG-3′; Reverse: 5′-AAC CAT GCC TAT CAT CCT TTG G-3′.

Cre: Forward 5′-GGC GTT TTC TGA GCA TAC CTG-3′; Reverse: 5′-CAT TCT CCC ACC GTC AGT ACG-3′.

For genotyping placentas and fetuses, a piece of tail from the fetus was processed using the standard gDNA extraction and PCR procedure, as described above. The genotype of the placenta can be determined by the genotype of the corresponding fetus.

2.3. Timed-mating for C57BL/6N wild-type, *Il6*$^{-/-}$, and *Cyp19-Cre*$^{+}$; *Il6a*$^{fl/fl}$ mutant mice

We adopted a trio timed-mating strategy (two female and one male) to minimize the number of sires and limit variation. The females were transferred to a clean cage one day before the introduced of the male into the cage. Timed-mating pairs were set up in the late phase of the light period. Vaginal plugs were checked the following morning. The day of vaginal plug presence was considered embryonic day 0.5 (E0.5). Three independent mouse lines were used in this study- C57BL/6N wild-type line, *Il6*$^{-/-}$ mutant line, and *Cyp19-Cre*$^{+}$;*Il6a*$^{fl/fl}$ mutant line. For the timed-mating of *Il6*$^{-/-}$ mutant line for Luminex cytokine array study, two kinds of breeding pairs were used- wild-type sire *x* *Il6*$^{-/-}$ dam and *Il6*$^{-/-}$ sire *x* wild-type dam. The genotype of offspring yielded from the two kinds of breeding pairs is *Il6*$^{+/-}$. For the timed-mating of *Cyp19-Cre*$^{+}$;*Il6a*$^{fl/fl}$ mutant line, the pair we used was *Il6ra*$^{fl/fl}$ sire x *Cyp19-Cre*$^{+}$;*Il6a*$^{fl/fl}$ dam. The genotype of offspring we yield from

Please cite this article in press as: Wu, W.-L., et al. The placental interleukin-6 signaling controls fetal brain development and behavior. Brain Behav. Immun. (2016), http://dx.doi.org/10.1016/j.bbi.2016.11.007

the breeding pair included *Il6ra*$^{fl/fl}$ and *Cyp19-Cre*$^{+}$;*Il6a*$^{fl/fl}$. All female mice were 8–16 weeks of age, with no prior pregnancies.

2.4. Maternal immune activation (MIA) by poly(I:C)

The induction of MIA is previously described (Chow et al., 2016). Briefly, Potassium salt poly(I:C) (P9582; Sigma, St. Louis, MO, USA) was used to induce MIA. 20 mg/kg poly(I:C) was dissolved in 0.9% sodium chloride (Hospira, Inc, Lake Forest, IL, USA). Either poly(I:C) or saline was intraperitoneally injected into pregnant mice on embryonic day 12.5 (E12.5). Poly(I:C) was prepared at 40 mg/ml of the actual weight of poly(I:C) powder.

2.5. Harvesting embryo and placenta at E12.5 from pregnant mice after MIA

Three hours (hr), 6 h or 24 h after poly(I:C) injection, mice were sacrificed by cervical dislocation without anesthesia. Placenta and fetal brains were harvested from poly(I:C)- and saline-injected pregnant mice, based on prior work in MIA on the placenta (Hsiao and Patterson, 2011). Fetal brains were dissected under a stereomicroscope (M5A, Wild Heerbrugg, Switzerland). For gene expression analysis, tissues were stored in RNAlater (Qiagen, Gaithersburg, MD, USA) at −80 °C until later used. For immunohistochemistry, fetal brains and placenta were postfixed in 4% paraformaldehyde at 4 °C for 30–60 min and then cryopreserved in 30% sucrose at room temperature overnight. Tissues were then embedded in OCT (Tissue-Tek, Torrance, CA, USA), frozen in 2-methybutane on dry ice and stored at −80 °C until used. For LCM, each embryo was immediately embedded in OCT and frozen in 2-methybutane on dry ice and stored at −80 degrees until used.

2.6. Harvesting adult brain for histology

Adult mice were euthanized using Euthasol. Mice were perfused via the cardiovascular system with PBS followed by 4% paraformaldehyde (Alfa Aesar, Ward Hill, MA, USA). Brains were removed and postfixed in 4% paraformaldehyde overnight at 4 °C. Postfixed brains were cryopreserved in 30% sucrose for 3 days at 4 °C and then embedded in OCT (Tissue-Tek, Torrance, CA, USA). The embedded brains were kept at −80 °C until sectioning.

2.7. RNA extraction and RT-PCR

RNA extraction of placenta and fetal brain was based on the manufacturer's protocol (Trizol; Life Technologies, Grand Island, NY, USA). The RNA concentration and quality were measured by NanoDrop (Thermo Scientific, Wilmington, DE, USA). Before reverse transcription, RNA was treated with DNase I (Promega, San Luis Obispo, CA, USA) to eliminate genomic DNA contamination. 1 μg RNA from each sample was reverse transcribed by using the iScript cDNA synthesis kit (Bio-Rad, Hercules, CA, USA).

2.8. Quantitative PCR (qPCR)

The gene expression of fetal brain subregions analysis was measured using Power SYBR Green PCR master mix (Life Technologies, Carlsbad, CA, USA) on ABI Prism 7900HT system (Life Technologies, Carlsbad, CA, USA). All other mRNA expression was measured using FastStart Universal SYBR Green master mix with ROX (Roche, El Cerrito, CA, USA) on the ABI 7300 real-time PCR system (Life Technologies, Carlsbad, CA, USA). Gene expression was normalized to β-actin mRNA. Data are presented as fold-change in gene expression in each group relative to that in the maternal saline control group. The primer sequences were adapted from the Harvard PrimerBank database (Spandidos et al., 2010).

2.9. Luminex cytokine array

Fetal brains were dissected at 3 h post-poly(I:C) injection and homogenized in Tissue Extraction Reagent I (Invitrogen, Life Technologies, Carlsbad, CA, USA) containing EDTA-free protease inhibitors (Roche, El Cerrito, CA, USA). For cytokine profiling, mouse 20-plex cytokine arrays (Invitrogen, Life Technologies, Carlsbad, CA, USA) were analyzed on the Luminex FLEXMAP 3D platform by the Clinical Immunobiology Correlative Studies Laboratory at the City of Hope (Duarte, CA). These cytokines, chemokines growth factors were chosen because of the relevance to the level of IL-6. Cytokine levels were normalized to total protein content as detected by BCA assay.

2.10. Cryosectioning

For fetal brain sectioning, whole embryos were sectioned sagittally at a thickness of 30 μm and adhered to a Superfrost Plus microscope slide (Fisher Scientific, Tustin, CA, USA). For placenta sectioning, placentas were cut sagittally at a thickness of 16 μm. Slides were stored at −80 °C until staining. For adult brain sectioning, 50 μm sagittal sections were cut at −20 °C and stored as free-floating in PBS at 4 °C until staining.

2.11. Immunohistochemistry

For colorimetric staining, the sections were postfixed with 4% paraformaldehyde for 10 min at room temperature. To eliminate endogenous peroxidase activity, the sections were incubated with 0.6% hydrogen peroxide (Sigma, St. Louis, MO, USA) for 30 min at room temperature. For pSTAT3 staining, antigen retrieval was conducted after endogenous peroxidase elimination. The slides were incubated in 10 mM sodium citrate pH 6.0 for 30 min in a 95 °C water bath. After incubation, slides were equilibrated to room temperature. To prevent non-specific binding of antibodies, the sections were incubated with blocking solution (10% goat serum, 0.1% triton X-100, and 0.02% sodium azide in PBS) for 1 h at room temperature. After blocking, the sections were incubated with primary antibody made in blocking solution overnight at room temperature. On the next day, the sections/slides were incubated with biotinylated secondary antibody for 2 h at room temperature. Lastly, the sections were incubated in VECTASTAIN ABC kit (Vector Laboratories Inc, Burlingame, CA, USA) for 1 h at room temperature and then developed using the VECTOR NovaRED peroxidase substrate kit (Vector Laboratories Inc, Burlingame, CA, USA) according to the manufacturer's instructions. Between each step, slides were thoroughly washed with PBS. The sections were dehydrated by xylene and then mounted with Permount mounting medium (Fisher Scientific, Tustin, CA, USA).

For fluorescence staining, the sections were postfixed with 4% paraformaldehyde for 10 min at room temperature. After fixation, the sections/slides were incubated in primary antibody made in blocking solution (10% horse serum, 0.1% triton X-100, and 0.02% sodium azide in PBS) overnight at room temperature. The next day, sections were incubated with fluorescence-conjugated secondary antibody for 2 h at room temperature. Between each step, sections were thoroughly washed with PBS. ProLong gold, anti-fade mounting medium (Molecular Probe, Life Technologies, Carlsbad, CA, USA) was applied to the slide before coverslip mounting.

Free-floating sections were mounted to Superfrost Plus microscope slides (Fisher Scientific, Tustin, CA, USA) after staining. For slide staining, a barrier was drawn on the edge of microscope slide by using ImmEdge Hydrophobic Barrier Pen (Vector Laboratories Inc, Burlingame, CA, USA).

The primary antibodies and their dilutions were rabbit anti-IL-6Rα (1:500; Santa Cruz, CA, USA), rabbit anti-Phosphorylation of

Please cite this article in press as: Wu, W.-L., et al. The placental interleukin-6 signaling controls fetal brain development and behavior. Brain Behav. Immun. (2016), http://dx.doi.org/10.1016/j.bbi.2016.11.007

the transcription factor Signal Transducer and Activator of Transcription 3 (pSTAT3; 1:500; Cell Signaling, Danvers, MA, USA), mouse anti-NeuN (1:500; Millipore, Darmstadt, Germany), rabbit anti-GFAP (1:500; DAKO, Glostrup, Denmark), rabbit anti-calbindin (1:1000; Abcam, Cambridge, MA, USA), mouse anti-GAD67 (1:1000; Millipore, Darmstadt, Germany), mouse anti-parvalbumin (1:1000; Sigma, St. Louis, MO, USA). The fluorescence-conjugated secondary antibodies were donkey anti-rabbit (1:1000), and donkey anti-mouse (1:1000) (all from Molecular Probes, Life Technologies, Carlsbad, CA, USA). The biotinylated secondary antibody was biotinylated goat anti-rabbit IgG antibody (1:200; Vector Laboratories Inc, Burlingame, CA, USA). Colorimetric staining images were taken using the Nikon DIAPHOT 300 (Nikon, Tokyo, Japan) with SPOT software (V4.6, Sterling Heights, MI, USA). Confocal imaging was done using the Zeiss LSM 5 Exciter inverted laser scanning microscope (Carl Zeiss MicroImaging Gmbh, Jena, Germany) with Zen 2009 software (Carl Zeiss MicroImaging Gmbh, Jena, Germany). Quantification of pSTAT3, calbindin, and parvalbumin positive cells was analyzed using ImageJ software (NIH, Bethesda, MD, USA).

For quantification of pSTAT3+ cells in placental spongiotrophoblast, the region of interest (ROI) was first selected by a segmented line. All images were converted to 8 bit, thresholds were set between 2.71 and 0.37 after calibration. The optical density for the ROI was analyzed by measurement of area fraction. The final value of optical density for each sample is and average of 5–6 sections. For the quantification of pSTAT3$^+$ cells in fetal brain, positive cells were manually counted by the cell counter from serial sections of whole fetal brains. The final number of positive cells is an average of multiple sections. For quantification of calbindin$^+$ and parvalbumin$^+$ cells in adult cerebellar lobule VII, confocal images for each sample were collected from different focal planes with 2.5 μm intervals, converted to Z-stacks and merged into a 2D image by maximum pixel intensity using Zen 2009 software. Positively stained cells were quantified using a manual cell counter. Cerebellum sections for each mouse were collected every 0.2 mm. The coordination for lobule VII quantification was from medial to lateral (ML) −0.04 mm to 1.20 mm relative to Bregma (bilateral). The length of the Purkinje cell layer was measured by a segmented line and further calibrated to the actual length. The final number of positive cells reported is averaged from multiple sections.

2.12. X-gal staining

Brain sections were incubated with rinse buffer (pH 7.3 100 mM sodium phosphate, 2 mM MgCl2, 0.01% sodium deoxycholate, 0.02% NP-40) 3 times for 40 min at room temperature. After rinsing, sections were stained in the rinse solution containing 5 mM potassium ferricyanide, 5 mM potassium ferrocyanide, and 1 mg/ml X-gal (from 25 mg/ml stock in dimethylformamide) for 24 h. After staining, sections were postfixed in 4% paraformaldehyde for 10 min at room temperature.

2.13. Laser capture microdissection (LCM) and transcriptome amplification

Fetal brains were cut into 16 μm sections on PALM Membrane Slides (415190-9081-000, MembraneSlide, Carl Zeiss, North York, ON, Canada). Cryostat blades and workstations were cleaned with RNaseZap (Applied Biosystems, Life Technologies, Carlsbad, CA, USA) to prevent RNA degradation. 10 sagittal sections were used for LCM. Duration was limited to < 30 min per slide to prevent RNA degradation. For each fetal brain section, the hindbrain was localized by morphology under the Axio Observer.Z1 confocal microscope (Zeiss; Thornwood, NY). Conservative regions of interest encompassing approximately 100 cell nuclei were microdissected (energy: 50–53; focus: 73) using the PALM Microbeam system and PALMRobo software 4.3 (Zeiss; Thornwood, NY) and immediately catapulted into an AdhesiveCap 200 microcentrifuge tube (415190-9181-000, Carl Zeiss, North York, ON, Canada Zeiss). RNA isolation was performed immediately as described above, with the RNeasy Micro Plus kit (Qiagen, Gaithersburg, MD, USA). Genomic DNA was removed using gDNA eliminator columns (Qiagen, Gaithersburg, MD, USA). Total RNA was amplified and reverse-transcribed using the QuantiTect Whole Transcriptome Amplification kit (Qiagen, Gaithersburg, MD, USA). 100 ng cDNA was used for qPCR, according to the methods described above.

2.14. Behavior

2.14.1. Experimental procedures

All mice that underwent behavior testing were maintained under the same conditions as described in Section 2.1. Mice were weaned at the age of 3 weeks. There is no significant difference in litter sizes across treatment groups (Saline: 7.3 ± 1.2 offspring, MIA: 7.3 ± 2.2 offspring) and sex ratios across treatment groups (Saline *Cre*$^-$: Male 1.8 ± 0.8, Female 1.4 ± 1.1; Saline *Cre*$^+$: Male 2.8 ± 1.5, Female 1.6 ± 1.1; MIA *Cre*$^-$: Male 1.9 ± 2.3, Female 1.9 ± 1.9; MIA *Cre*$^+$: Male 1 ± 1.7, Female 2.6 ± 2.1). Both male and female mice were behaviorally tested (male female ratio is 1:1). The male mice were tested prior to female mice in order to avoid the interference of female scent. All behavior tests were performed at 13:00-19:00 daily. The experimenter was blinded from the genotypes while performing behavioral testing and analyzing behavioral data.

2.14.2. Timeline

Marble burying was performed at 7 weeks of age. The 3-chamber social test was performed at 8 weeks of age. All the apparatuses were cleaned with 70% ethanol and then tap water between subjects. Cage bedding was not changed 3 days prior to behavioral testing. Mice were acclimated to the testing room at least 30 min before each behavior test.

2.14.3. Three-chamber social test

The design and procedure for the 3-chamber social test was modified from previous literature (Yang et al., 2011, chap. 8). The social chamber is a 40 (width) × 20 (length) × 22 (height) cm Plexiglas box divided equally into 3-chambers by transparent walls made by Plexiglas with the opening doors (10 cm width × 5 cm height). The procedure consisted of two consecutive phases- habituation and sociability. In habituation phase, mouse was placed in the center of the social chamber for 10 min and allowed to freely explore each compartment. In the sociability phase, the testing mouse was enclosed in the center compartment of social chamber with the doors closed. Two inverted steel wire cups were placed in each of the two side chambers. An unfamiliar, strain-, age- and gender- matched mouse was placed in one of the inverted wire cups. The unfamiliar mice were purchased from Jackson Laboratory (Bar Harbor, ME, USA). The other inverted wire cup represented a novel object. After setting up, the doors were opened, and the mouse was allowed to investigate the chamber for 10 min. The behavior was recorded by a video camera mounted above the apparatus. Ethovision (Noldus Information Technology, Leesburg, VA, USA) was used to analyze the duration of the mouse in each chamber. Mice were only excluded from the data if they showed biased preference to a certain side of chamber during habituation phase.

Please cite this article in press as: Wu, W.-L., et al. The placental interleukin-6 signaling controls fetal brain development and behavior. Brain Behav. Immun. (2016), http://dx.doi.org/10.1016/j.bbi.2016.11.007

2.14.4. Marble burying test

Marble burying is a test for repetitive behavior. The procedure has been previously described (Malkova et al., 2012) with modification. The mouse was first acclimated to a test cage with compressed, 5-cm deep clean, Aspen pine bedding. After this habituation the mouse was returned to its home cage. 20 navy blue glass marbles (15 mm diameter) were gently placed on the bedding of the test cage (4 × 5 arrangement). The mouse was then returned to this test cage and, after 10 min, the number of buried marbles was counted. The criteria for a buried marble was over 50% of the marble covered by bedding. The marbles were cleaned with 70% alcohol, dried, and submerged in Aspen pine bedding between each test.

2.15. Statistic analysis

All data are represented as mean ± standard error mean (SEM). The fetus/offspring used for qRT-PCR, cytokine array, immunohistochemistry were collected from at least 3 independent litters per group. The offspring used for behavior testing were pooled from at least from 6 independent litters (l) per group. The data were analyzed by using a litter as an n number in order to minimize potential confounding litter effect. All offspring were used for each litter. Specifically, the readouts of the offspring from each litter were averaged and used the averaged number to be the biological replicate (Wu et al., 2015). Analysis with the two-tailed unpaired *t* test was used to compare data between two groups. Data with two variable factors were analyzed by two-way ANOVA with *post hoc* test. The data analyzed using Prism 6.0 (Graphpad, La Jolla, CA, USA). *p* value is used to justify the significance between groups. When *p* is smaller than 0.05, the groups are considered as different. The number of asterisks indicates the difference in the figures.

3. Results

3.1. Increased IL-6 gene expression levels in MIA fetal brain

To determine the temporal pro-inflammatory responses of MIA on the developing offspring, we analyzed fetal brain *Il6* gene expression at different time point after injection of poly(I:C) to dams at E12.5. Brain *Il6* levels are higher in fetuses from poly(I:C)-treated dams compared to saline treated dams at 3 h post-injection (Fig. 1A). *Il6* levels return to baseline at 6 and 24 h post-poly(I:C) injection (Fig. 1A). Thus, the rapid and transient elevation of *Il6* gene expression in fetal brain represents an acute inflammatory insult to the developing fetus.

3.2. The transcription factor STAT3 and downstream signaling are activated in the hindbrain of the MIA fetus

pSTAT3 is a downstream activation marker of cytokine signaling. Immunohistochemistry analysis of pSTAT3 in the brain of embryos at 3 h post- poly(I:C) injection revealed spatially restricted immune activation following MIA. Several central and peripheral areas in the fetus display positive pSTAT3 staining, including the hindbrain, trigeminal ganglion (Fig. 1B, Supplementary Fig. S1–S3). The most dramatic changes in pSTAT3 levels are in hindbrain areas—specifically the prepontine hindbrain (PPH) and pontine hindbrain (PH) (Fig. 1B, low magnification in Supplementary Fig. S1A and detailed annotation in Fig. S1B). These two hindbrain areas develop into the cerebellum and brainstem (Puelles et al., 2013), sites of dysfunction in some cases of autism (Courchesne, 1997; Rodier et al., 1996; Wang et al., 2014). The distribution of pSTAT3$^+$ cells is significantly higher in the MIA fetal brain compared to saline controls within the PPH and PH (Fig. 1C), and largely localize to the lateral side of the fetal brain.

To further analyze regional-specific pro-inflammatory responses identified by pSTAT3 staining, we collected the PH by LCM (Supplementary Fig. S1C), and examined the expression of genes relevant to the JAK/STAT3 signaling pathway. Following MIA induction, *Stat3* and *Myc* expressions are significantly increased in the PH (Fig. 1D). This is consistent with the finding that *Myc* is a central "hub" in signaling pathways enriched in the ASD brain (Ziats and Rennert, 2011). Taken together, these data reveal that MIA induces increased cytokines expression and activation of STAT3 signaling pathways within specific brain regions in the developing fetus.

3.3. Maternal IL-6 is required for immune activation in the fetal brain during MIA

Based on the finding that IL-6 is induced directly in the fetal brain following MIA, in addition to previous reports revealing that MIA elevates IL-6 in the maternal blood and placenta, we aimed to determine whether maternal IL-6 is required for the priming of acute inflammatory response in the fetal brain. Wild-type male mice were crossed to *Il6*$^{-/-}$ females and, in parallel, *Il6*$^{-/-}$ males were crossed to wild-type females. MIA was induced in pregnant females, generating *Il6*$^{+/-}$ MIA offspring in both cases. IL-6, IL-4, and IP-10 protein levels are increased in the *Il6*$^{+/-}$ fetal brain of offspring from wild-type females that have been injected with poly (I:C), compared to saline controls (Fig. 1E). Furthermore, elevation of IL-6, IL-4, and IP10 in the *Il6*$^{+/-}$ fetal brain were not observed upon injection of poly(I:C) into *Il6*$^{-/-}$ females, indicating that maternal sources of IL-6 are required for acute induction of cytokines in the fetal brain after MIA. In addition, maternal IL-6 is required for maintaining baseline levels of FGF-basic, IL-2, IL-12p40/p70, KC, and VEGF. These data demonstrate that IL-6 protein expression in the mother exacerbates an inflammatory program in the fetus that may impact brain function and development. Though this finding does not rule out a role for IL-6 signaling outside the fetal brain, it prompted us to examine how IL-6 at the maternal-fetal interface transmits immune activation and behavioral deficits to the fetus.

3.4. Generation of placental trophoblast Il6ra conditional knockout mice

To validate *Cyp19-Cre* recombinase-mediated *Il6ra* deletion, we analyzed mRNA and protein levels for the IL-6Rα in the placenta. Analysis of whole placenta RNA extracts from the *Cyp19-Cre*$^+$;*Il6ra*$^{fl/fl}$ group shows a ~50% reduction in the *Il6ra* transcript level compared to the *Il6ra*$^{fl/fl}$ group, regardless of MIA induction, which indicates that *Cyp19-Cre* is specifically localized at SP layer, instead of whole placenta (Fig. 2A). Antibody staining of placental tissue sections for IL-6Rα shows minimal expression in the SP layer of *Cyp19-Cre*$^+$;*Il6ra*$^{fl/fl}$ mice. In contrast, a few IL-6Rα$^+$ cells can be detected in SP layer of the saline control and placenta from MIA-treated *Il6ra*$^{fl/fl}$ offspring (Supplementary Fig. S4). In addition, knockout of *Il6ra* does not alter *Il6* gene expression in the placenta, as elevation of *Il6* is detected in MIA mice regardless of receptor expression (Fig. 2B). To confirm that *Cyp19-Cre* is not residually expressed directly in the brain, we evaluated β-galactosidase expression in the brains of *Cyp19-Cre*$^+$;*ROSA::LSL-lacZ* mice. β-galactosidase staining is absent in the brains of *Cyp19-Cre*$^+$;*ROSA::LSL-lacZ* mice, while the positive control shows strong expression across different brain regions (Supplementary Fig. S5). Moreover, IL-6Rα is intact in the calbindin$^+$ cerebellar Purkinje cells and brainstem motor trigeminal nucleus (MO5) of *Cyp19-Cre*$^+$;*Il6ra*$^{fl/fl}$ brains (Supplementary Fig. S6). No difference is

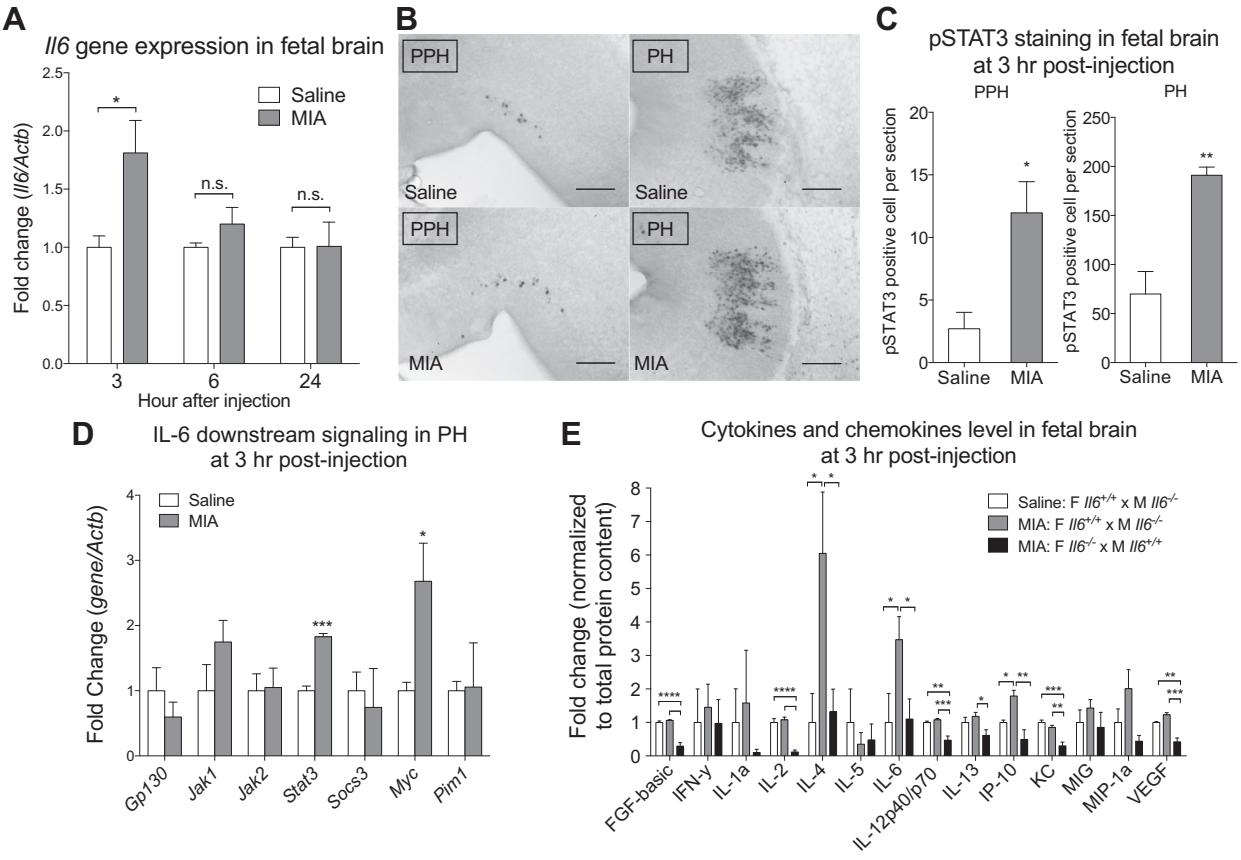

Fig. 1. MIA induces an acute immune response in the fetal brain. (A) The level of IL-6 in fetal brain was measured by qPCR. Fetal brains from poly(I:C)-injected dam exhibit elevated *Il6* gene expression at 3 h post-injection ($t_{10} = 2.732$, $p = 0.0211$; Student's two-tailed unpaired t test). No difference in *Il6* gene expression is observed between saline and MIA fetal brains at 6 and 24 h post-injection. (3 h: Saline n = 6 l (16 embryos); MIA n = 6 l (18 embryos); 6 h and 24 h: Saline n = 3 l (9 embryos); MIA n = 3 l (9 embryos). *Il6* gene expression was normalized to *β-actin*. (B) pSTAT3 is increased in MIA fetal hindbrain at 3 h post-poly(I:C) injection. Representative images of pSTAT3 staining in sagittal sections of the MIA fetal prepontine hindbrain (PPH) and pontine hindbrain (PH). Scale bar = 200 μm. (C) Quantification of pSTAT3$^+$ cells in the fetal PPH ($t_7 = 3.038$, $p = 0.0189$) and PH ($t_6 = 3.888$, $p = 0.0081$) (Student's two-tailed unpaired t test). Saline n = 4 l (7 embryos); MIA n = 5 l (5 embryos). (D) Downstream signaling molecules of the IL-6 pathway in fetal MIA and control LCM samples are analyzed by qPCR. The results are normalized to *β-actin* using the ddCT method. *Stat3* ($t_4 = 9.483$, $p = 0.0007$) and *Myc* ($t_4 = 2.810$, $p = 0.0483$) expression are significantly increased in the PH area after MIA (Student's two-tailed unpaired t test). Saline n = 3 l (7–9 embryos); MIA n = 3 l (9–10 embryos). (E) Luminex cytokine array indicates that MIA-mediated alterations in fetal brain cytokines and chemokines depend on maternal IL-6 genotype. *White bars* represent cytokine levels in *Il6*$^{+/-}$ fetal brains collected from wild-type females that were mated to *Il6*$^{-/-}$ males and injected with saline. *Gray bars* represent cytokine levels in *Il6*$^{+/-}$ fetal brains collected from wild-type females that were mated to *Il6*$^{-/-}$ males and injected with poly(I:C). *Black bars* represent cytokine levels in *Il6*$^{+/-}$ fetal brains collected from *Il6*$^{-/-}$ females that were mated to wild-type males and injected with poly(I:C). Values were normalized to white bar. Data shows that maternal poly(I:C) injection induces cytokine levels in fetal brain and that maternal IL-6 is required for induction of fetal brain IL-4 (Saline WT dam v.s. MIA WT dam $p = 0.0176$; MIA WT dam v.s. MIA KO dam $p = 0.0238$), IL-6 (Saline WT dam v.s. MIA WT dam $p = 0.0397$; MIA WT dam v.s. MIA KO dam $p = 0.0465$), IP-10 (Saline WT dam v.s. MIA WT dam $p = 0.0201$; MIA WT dam v.s. MIA KO dam $p = 0.0012$) and for maintaining baseline levels of FGF-basic (Saline WT dam v.s. MIA KO dam $p < 0.0001$; MIA WT dam v.s. MIA KO dam $p < 0.0001$), IL-2 (Saline WT dam v.s. MIA KO dam $p < 0.0001$; MIA WT dam v.s. MIA KO dam $p < 0.0001$), KC (Saline WT dam v.s. MIA KO dam $p = 0.0002$; MIA WT dam v.s. MIA KO dam $p = 0.0012$), VEGF (Saline WT dam v.s. MIA KO dam $p = 0.0004$; MIA WT dam v.s. MIA KO dam $p < 0.0001$) (One-way ANOVA with Fisher's LSD *post hoc* test). All groups n = 4 l (4 embryos per group). Cytokine levels were normalized to total protein content. $^*p < 0.05$, $^{**}p < 0.01$, $^{***}p < 0.001$, $^{****}p < 0.0001$ v.s. saline control. Data are presented as mean ± SEM. n.s.: not significant.

observed in the global distribution of neurons and astrocytes across various adult brain regions in *Cyp19-Cre*$^+$;*Il6ra*$^{fl/fl}$ offspring compared to *Il6ra*$^{fl/fl}$ offspring (Supplementary Fig. S7). Further, there are no differences in body weights between *Cyp19-Cre*$^+$; *Il6ra*$^{fl/fl}$ and *Il6ra*$^{fl/fl}$ offspring (Supplementary Fig. S8).

3.5. Knockout of placental trophoblast Il6ra blocks MIA induced pSTAT3 activation in spongiotrophoblast layer and placental Prl2b1 gene expression

pSTAT3 is increased in the placenta 3 h post-poly(I:C) injection, with a maternal IL-6 dependent activation of pSTAT3 in the SP layer (Hsiao and Patterson, 2011). We observed the same effect in MIA-induced *Il6ra*$^{fl/fl}$ mice, as the distribution of pSTAT3$^+$ cells dramatically increase in the SP layer of MIA *Il6ra*$^{fl/fl}$ placentas compared to saline controls, while this increase is not observed in *Cyp19-Cre*$^+$;*Il6ra*$^{fl/fl}$ mice (Fig. 2C and E). Furthermore, knockout of *Il6ra* in the placental trophoblasts blocks pSTAT3 activation in the SP layer of the placenta following MIA treatment, but not in saline controls (Fig. 2C and E). To corroborate the observation that IL-6 signaling is inhibited in the placenta of these mice, levels of *Prl2b1* (Prolactin family 2 subfamily b member 1 hormone) were also examined. *Prl2b1* is a placenta specific protein expressed in multiple trophoblast lineages (Dai et al., 2000), and we previously demonstrated that *Prl2b1* expression is elevated in the placenta of poly(I:C)-treated dams, in a maternal IL-6-dependent manner (Hsiao and Patterson, 2011). An interaction of *Cre* and MIA is detected in *Prl2b1* expression (Fig. 2D). *Il6ra*$^{fl/fl}$ and *Cyp19-Cre*$^+$; *Il6ra*$^{fl/fl}$ do not differ in placental *Prl2b1* expression in saline treated groups; however, for the MIA treatment, *Prl2b1* expression is significantly lowered in *Cyp19-Cre*$^+$;*Il6ra*$^{fl/fl}$ compared to *Il6ra*$^{fl/fl}$ placenta. In addition, in the *Il6ra*$^{fl/fl}$ placenta, *Prl2b1* expression is increased in the MIA treated group. Within the *Cyp19-Cre*$^+$;*Il6ra*$^{fl/fl}$ placenta, there is no difference between saline and MIA groups.

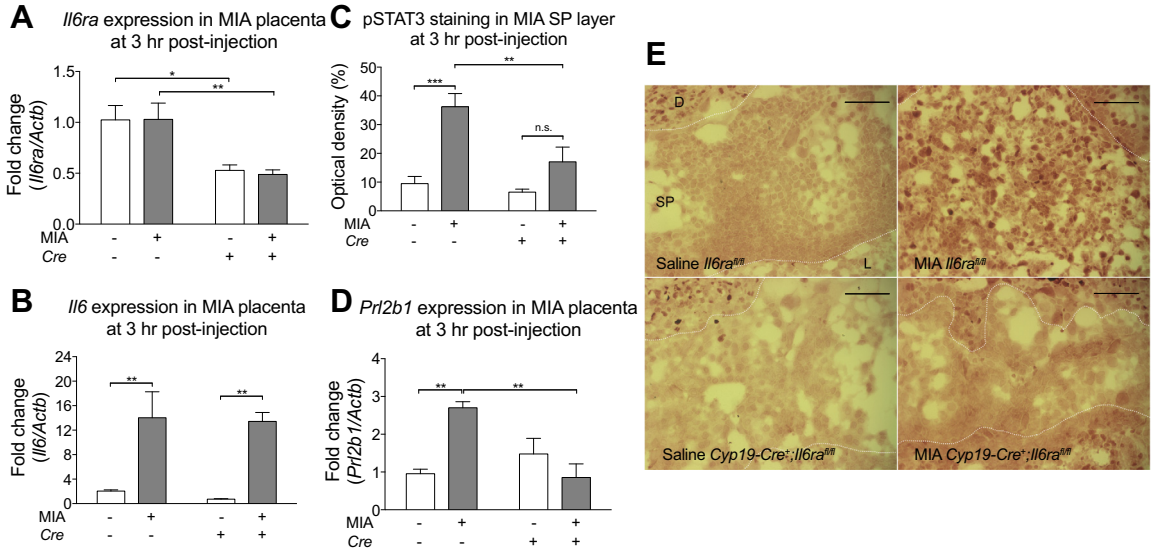

Fig. 2. Deletion of placental trophoblast *Il6ra*$^{fl/fl}$ decreases STAT3 activation, but not IL-6 production after MIA. (A) The level of IL-6Rα in placenta was measured by qPCR. *Il6ra* expression is decreased in the *Cyp19-Cre*$^{+}$;*Il6ra*$^{fl/fl}$ placenta. There is no effect of MIA on placental *Il6ra* expression. All groups n = 3 l (6, 9, 4, 8 placentas were used for Saline *Cre*$^{-}$; MIA *Cre*$^{-}$; Saline *Cre*$^{+}$; MIA *Cre*$^{+}$, respectively) (MIA: $F_{(1,8)} = 0.08604$, $p = 0.8774$; Cre: $F_{(1,8)} = 72.66$, $p = 0.0017$; MIAxCre: $F_{(1,8)} = 0.1413$, $p = 0.8433$; *Post hoc*- *Cre*$^{-}$ v.s. *Cre*$^{+}$: Saline $p = 0.0140$, MIA $p = 0.0091$) (Two-way ANOVA with Fisher's LSD *post hoc* test). (B) The level of IL-6 in placenta was measured by qPCR. MIA increases *Il6* gene expression in both *Il6ra*$^{fl/fl}$ and *Cyp19-Cre*$^{+}$;*Il6ra*$^{fl/fl}$ placentas. There is no effect of *Il6ra* genotype on placental *Il6* gene expression in response to MIA. All groups n = 3 l (6, 9, 4, 8 placentas were used for Saline *Cre*$^{-}$; MIA *Cre*$^{-}$; Saline *Cre*$^{+}$; MIA *Cre*$^{+}$, respectively) (MIA: $F_{(1,8)} = 78.65$, $p = 0.0006$; Cre: $F_{(1,8)} = 0.4826$, $p = 0.6780$; MIAxCre: $F_{(1,8)} = 0.06658$, $p = 0.8768$; *Post hoc*- Saline v.s. MIA: *Cre*$^{-}$ $p = 0.0054$, *Cre*$^{+}$ $p = 0.0039$) (Two-way ANOVA with Fisher's LSD *post hoc* test). (C) Quantification of pSTAT3 optical density in the placental spongiotrophoblast (SP) layer. All groups n = 3 l (3 placentas per group). (MIA: $F_{(1,8)} = 25.34$, $p = 0.001$; Cre: $F_{(1,8)} = 8.906$, $p = 0.0175$; MIAxCre: $F_{(1,8)} = 4.794$, $p = 0.06$; *Post hoc*- Saline v.s. MIA: *Cre*$^{-}$ $p = 0.0009$, *Cre*$^{+}$ $p = 0.0791$; *Cre*$^{-}$ v.s. *Cre*$^{+}$: Saline $p = 0.5895$, MIA $p = 0.0064$) (Two-way ANOVA with Fisher's LSD *post hoc* test) (D) The level of Prolactin family 2 subfamily b member 1 hormone in placenta was measured by qPCR. MIA increases *Prl2b1* expression in the *Il6ra*$^{fl/fl}$ placenta. This elevation is prevented in placentas from MIA *Cyp19-Cre*$^{+}$;*Il6ra*$^{fl/fl}$ mice. All groups n = 3 l (5, 6, 5, 6 placentas were used for Saline *Cre*$^{-}$; MIA *Cre*$^{-}$; Saline *Cre*$^{+}$; MIA *Cre*$^{+}$, respectively) (MIA: $F_{(1,8)} = 3.657$, $p = 0.0922$; Cre: $F_{(1,8)} = 5.159$, $p = 0.0528$; MIAxCre: $F_{(1,8)} = 16.58$, $p = 0.0036$; *Post hoc*- Saline v.s. MIA: *Cre*$^{-}$ $p = 0.0029$, *Cre*$^{+}$ $p = 0.1653$; *Cre*$^{-}$ v.s. *Cre*$^{+}$: Saline $p = 0.2388$, MIA $p = 0.0020$) (Two-way ANOVA with Fisher's LSD *post hoc* test). (E) Representative images of pSTAT3 in the SP layer of saline *Il6ra*$^{fl/fl}$, MIA *Il6ra*$^{fl/fl}$, saline *Cyp19-Cre*$^{+}$;*Il6ra*$^{fl/fl}$, and MIA *Cyp19-Cre*$^{+}$;*Il6ra*$^{fl/fl}$ placentas. Scale bar = 100 μm. Gene expression was normalized to *β-actin*. $^{*}p < 0.05$, $^{**}p < 0.01$, $^{***}p < 0.001$ between groups. Data are presented as mean ± SEM. D: decidua, L: labyrinth, n.s.: not significant.

Overall, these experiments confirm that knockout of IL-6Rα in the placental trophoblast abolishes IL-6-dependent responses in placental pSTAT3 activation and downstream gene expression.

3.6. Inhibition of placental IL-6 signaling prevents immune responses in the fetal brain

To determine whether placental IL-6 signaling after MIA is required for the elevated *Il6* gene expression observed in fetal brain, we analyzed the pro-inflammatory response in fetal brains of *Cyp19-Cre*$^{+}$;*Il6ra*$^{fl/fl}$ mice. Gene expression analysis shows that *Il6* gene expression is increased in *Il6ra*$^{fl/fl}$ fetal brains after MIA induction, but not in *Cyp19-Cre*$^{+}$;*Il6ra*$^{fl/fl}$ fetal brains (Fig. 3A). pSTAT3 activation in the fetal brain is also reduced following inhibition of IL-6 signaling in the placenta (Fig. 3B–E). Specifically, within the fetal PPH, a main effect for *Cre* and an interaction for *Cre* and MIA are detected in fetal brain pSTAT3 activation. Knockout of trophoblast *Il6ra* results in the reduction of pSTAT3^{+} cells in the fetal PPH following MIA induction. However, the distribution of pSTAT3^{+} cells in the fetal PPH is not different between *Il6ra*$^{fl/fl}$ and *Cyp19-Cre*$^{+}$;*Il6ra*$^{fl/fl}$ fetuses in saline controls (Fig. 3B and D). In addition, for *Il6ra*$^{fl/fl}$ fetal brains, MIA increases the distribution of pSTAT3^{+} cells in the PPH; however, in *Cyp19-Cre*$^{+}$;*Il6ra*$^{fl/fl}$ fetal brains, numbers of pSTAT3^{+} cells for saline and MIA are similar. Within the fetal PH, knockout of trophoblast *Il6ra* results in the reduction of pSTAT3^{+} cells in both saline and MIA groups (Fig. 3C and E). There is no difference in pSTAT3^{+} cells in the PH between saline and MIA in both *Il6ra*$^{fl/fl}$ and *Cyp19-Cre*$^{+}$;*Il6ra*$^{fl/fl}$ fetal brains. These data reveal that MIA-induced IL-6 signaling at the maternal-fetal interface of the placenta leads to activation of the immune system within the fetal brain.

3.7. Knockout of placental Il6ra prevents cerebellum neuropathology in the MIA offspring

Loss of Purkinje cells in lobule VII of the cerebellum is one of the neuropathological phenotypes seen in the MIA model as well as in ASD (Naviaux et al., 2013; Shi et al., 2009; Skefos et al., 2014). To determine whether inhibition of placental trophoblast IL-6 signaling can prevent the loss of Purkinje cell in adulthood, we visualized calbindin^{+} Purkinje cells in adult brain sections from control and placental trophoblast IL-6Rα deficient offspring born to immune-activated mothers. A reduction in calbindin^{+} Purkinje cells was observed in the cerebellar lobule VII of *Il6ra*$^{fl/fl}$ offspring following MIA compared to saline *Il6ra*$^{fl/fl}$ controls (Fig. 4A and A′). The reduction of calbindin^{+} Purkinje cells in the cerebellar lobule VII by MIA is not observed in *Cyp19-Cre*$^{+}$;*Il6ra*$^{fl/fl}$ offspring (Fig. 4A″ and B). Due to an interaction of *Cre* and MIA, we further analyzed calbindin^{+} Purkinje cells between *Il6ra*$^{fl/fl}$ and *Cyp19-Cre*$^{+}$;*Il6ra*$^{fl/fl}$ offspring. Remarkably, for the MIA group, *Cyp19-Cre*$^{+}$;*Il6ra*$^{fl/fl}$ offspring display significantly greater densities of calbindin^{+} Purkinje cells in the cerebellar lobule VII compared to *Il6ra*$^{fl/fl}$ offspring (Fig. 4A′ and 4A‴). However, in saline control animals, calbindin^{+} Purkinje cells do not differ between *Il6ra*$^{fl/fl}$ and *Cyp19-Cre*$^{+}$;*Il6ra*$^{fl/fl}$ offspring (Fig. 4A and A″). These results suggest that elevated placental IL-6 signaling in response to MIA is required to perturb the neurodevelopment of Purkinje cells in lobule VII.

Dysfunction of inhibitory neurotransmission has been described in ASD patients and mouse models (Coghlan et al., 2012). To understand whether the inhibitory neurons of Purkinje cell populations are affected by MIA, we co-stained calbindin with the inhibitory neuronal markers – parvalbumin and glutamate decarboxylase 67 (GAD67). Co-staining indicates that Purkinje

Please cite this article in press as: Wu, W.-L., et al. The placental interleukin-6 signaling controls fetal brain development and behavior. Brain Behav. Immun. (2016), http://dx.doi.org/10.1016/j.bbi.2016.11.007

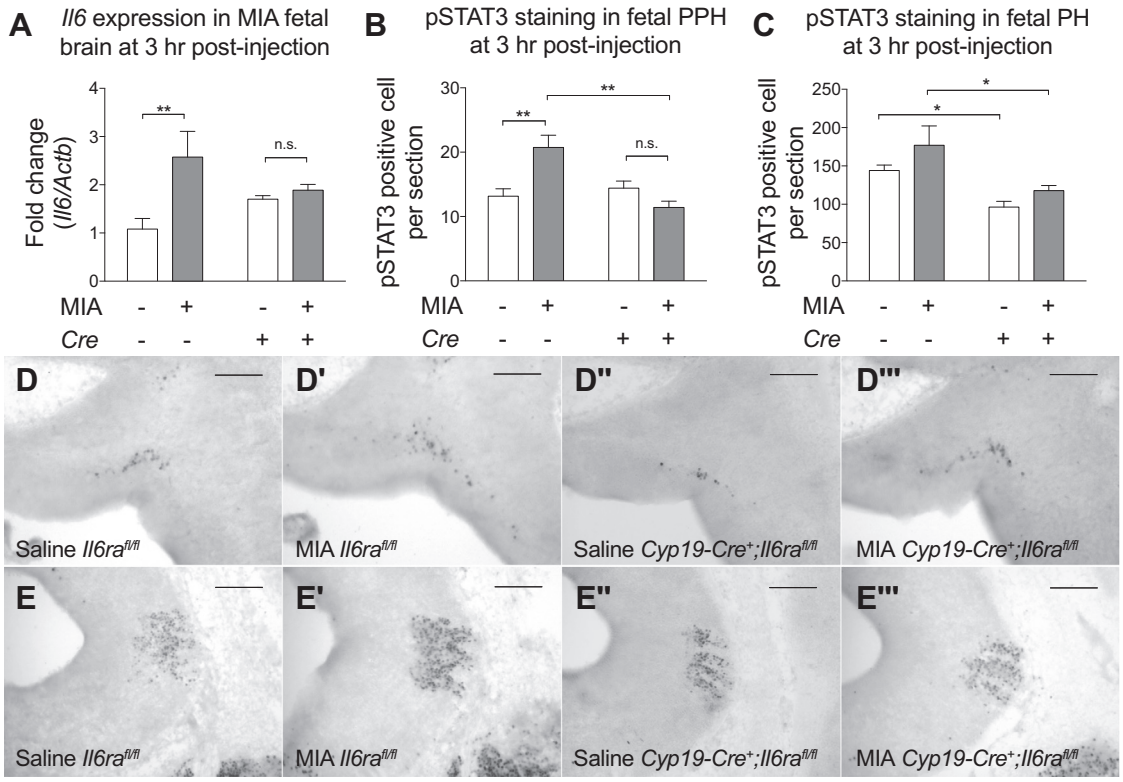

Fig. 3. Deletion of placental trophoblast *Il6ra* prevents MIA-induced acute responses in the fetal brain. (A) Fetal brain IL-6 gene expression was measured by qPCR. MIA increases *Il6* gene expression in the *Il6ra*$^{fl/fl}$ fetal brain, but not in *Cyp19-Cre*$^{+}$;*Il6ra*$^{fl/fl}$ fetal brain. *Il6* gene expression was normalized to *β-actin*. All groups n = 3 l (8, 7, 8, 12 fetal brains were used for Saline *Cre*$^{-}$; MIA *Cre*$^{-}$; Saline *Cre*$^{+}$; MIA *Cre*$^{+}$, respectively). (MIA: $F_{(1,8)} = 8.043$, $p = 0.0219$; Cre: $F_{(1,8)} = 0.01323$, $p = 0.9113$; MIAxCre: $F_{(1,8)} = 4.883$, $p = 0.0581$; *Post hoc*- Saline v.s. MIA: *Cre*$^{-}$ $p = 0.0073$, *Cre*$^{+}$ $p = 0.6696$) (Two-way ANOVA with Fisher's LSD *post hoc* test) (B and C) Quantification of pSTAT3^{+} cells in the fetal (B) prepontine hindbrain (PPH) (MIA: $F_{(1,8)} = 2.956$, $p = 0.1239$; Cre: $F_{(1,8)} = 9.251$, $p = 0.0160$; MIAxCre: $F_{(1,8)} = 15.96$, $p = 0.0040$; *Post hoc*- Saline v.s. MIA: *Cre*$^{-}$ $p = 0.0037$, *Cre*$^{+}$ $p = 0.1463$; *Cre*$^{-}$ v.s. *Cre*$^{+}$: Saline $p = 0.5192$, MIA $p = 0.0011$) and (C) pontine hindbrain (PH) (MIA: $F_{(1,8)} = 3.757$, $p = 0.0886$; Cre: $F_{(1,8)} = 14.50$, $p = 0.0052$; MIAxCre: $F_{(1,8)} = 0.1662$, $p = 0.6942$; *Post hoc*- *Cre*$^{-}$ v.s. *Cre*$^{+}$: Saline $p = 0.0429$, MIA $p = 0.0176$). All groups n = 3 l (6, 7, 3, 6 fetal brains were used in Saline *Cre*$^{-}$; MIA *Cre*$^{-}$; Saline *Cre*$^{+}$; MIA *Cre*$^{+}$, respectively) (Two-way ANOVA with Fisher's LSD *post hoc* test). pSTAT3^{+} cells are more abundant in MIA-induced in *Il6ra*$^{fl/fl}$ fetal PPH compared to saline controls. Reduction of pSTAT3^{+} cells in the fetal PPH is observed in *Cyp19-Cre*$^{+}$;*Il6ra*$^{fl/fl}$ compared to *Il6ra*$^{fl/fl}$ fetus following MIA. (D and E) Elevation of pSTAT3 in MIA fetal hindbrain is prevented when knockout of *Il6ra* in placental trophoblast. Representative images of pSTAT3 staining in sagittal sections of saline *Il6ra*$^{fl/fl}$, MIA *Il6ra*$^{fl/fl}$, saline *Cyp19-Cre*$^{+}$;*Il6ra*$^{fl/fl}$ and MIA *Cyp19-Cre*$^{+}$;*Il6ra*$^{fl/fl}$ fetal PPH (D) and PH (E). Scale bar = 200 μm. $^{*}p < 0.05$, $^{**}p < 0.01$ between groups. Data are presented as mean ± SEM. n.s.: not significant.

cells that express calbindin also express parvalbumin and GAD67 in lobule VII (Fig. 4A and Supplementary Fig. S9). Offspring whose mothers were treated with MIA not only contain fewer calbindin^{+} cells, but also display lower proportions of parvalbumin^{+} cells in the Purkinje cell layer (PCL) of lobule VII. This reduction is more pronounced in *Il6ra*$^{fl/fl}$ offspring (Fig. 4A and C). In addition, although an interaction of *Cre* and MIA is detected, there is no detectable difference between *Il6ra*$^{fl/fl}$ and *Cyp19-Cre*$^{+}$;*Il6ra*$^{fl/fl}$ offspring in both saline and MIA groups (Fig. 4A and C). The reduction of parvalbumin^{+} cells by MIA is restricted to the PCL, whereas parvalbumin^{+} cells are intact in molecular layer (ML) of the cerebellum (Fig. 4A). There is no detectable difference in GAD67 staining in the PCL between offspring of saline and MIA *Il6ra*$^{fl/fl}$ mice (Supplementary Fig. S9). Collectively, these data show that activation of the IL-6 pathway in the placenta leads to MIA-induced Purkinje cell defects in offspring, a neuropathology also found in ASD.

3.8. Knockout of placental Il6ra prevents behavioral abnormalities in the MIA model

MIA offspring exhibit behavioral abnormalities relevant to ASD (Hsiao et al., 2013). Here, we reveal that placental IL-6 signaling during gestation is a key mediator of MIA-induced impairments in social and marble burying behaviors (Fig. 5A–C). In the 3-chamber social test, the time spent in mouse chamber (social) and object chamber (asocial) is not different in MIA *Il6ra*$^{fl/fl}$ mice (Fig. 5A), whereas offspring in other group spend more time in the mouse chamber compared to the object chamber (Fig. 5A). Similarly, when we further analyzed the investigation time toward stranger mouse and object, MIA *Il6ra*$^{fl/fl}$ offspring have no preference in investigating a stranger mouse and an object (Fig. 5B), whereas other groups investigate the stranger mouse more than object (Fig. 5B). Thus, placental IL-6 signaling impacts social interaction in offspring. Finally, in the marble burying paradigm for repetitive/stereotyped behavior, an interaction of *Cre* and MIA is detected in marble burying behavior. Following MIA treatment, knockout of placental *Il6ra* results in the reduction of offspring marble burying behavior when compared to *Il6ra*$^{fl/fl}$ offspring. However, for the saline treatment groups, marble burying behavior does not differ between *Cyp19-Cre*$^{+}$;*Il6ra*$^{fl/fl}$ and *Il6ra*$^{fl/fl}$ offspring (Fig. 5C). Furthermore, MIA results in the increase of marble burying behavior in *Il6ra*$^{fl/fl}$ offspring, whereas MIA has no effect on marble burying behavior in *Cyp19-Cre*$^{+}$;*Il6ra*$^{fl/fl}$ offspring (Fig. 5C). In addition, no sexual dimorphism in MIA-related behavioral abnormalities was observed in *Cyp19-Cre*$^{+}$;*Il6ra*$^{fl/fl}$ offspring (Supplementary Fig. S10). These results indicate that placental IL-6 signaling is required for MIA-induced behavioral abnormalities in social and marble burying behaviors.

4. Discussion

The ASD risk factor, MIA, initiates an immunologic program that leads to offspring with abnormalities in fetal brain development

Please cite this article in press as: Wu, W.-L., et al. The placental interleukin-6 signaling controls fetal brain development and behavior. Brain Behav. Immun. (2016), http://dx.doi.org/10.1016/j.bbi.2016.11.007

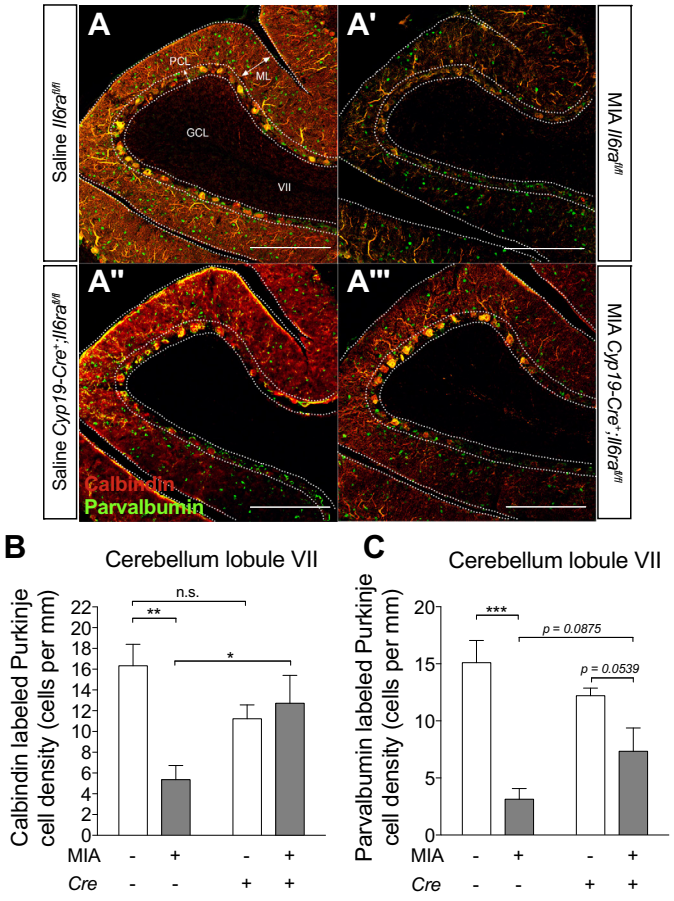

Fig. 4. Deletion of placental trophoblast *Il6ra* prevents cerebellar neuropathology and behavioral abnormalities in MIA offspring. (A) Representative images of calbindin and parvalbumin immunofluorescence staining in the offspring adult brain. Cerebellar Purkinje cells are labeled by calbindin (red) and co-stained for parvalbumin (green). Scale bar = 200 μm. Quantification of (B) calbindin$^+$ and (C) parvalbumin$^+$ Purkinje cell density at cerebellar lobule VII (Calbindin- MIA: $F_{(1,8)} = 24.14$, $p = 0.0410$; Cre: $F_{(1,8)} = 1.392$, $p = 0.5752$; MIAxCre: $F_{(1,8)} = 41.85$, $p = 0.0126$; *Post hoc*- Saline v.s. MIA: *Cre*$^-$ $p = 0.0040$, *Cre*$^+$ $p = 0.6008$; *Cre*$^-$ v.s. *Cre*$^+$: Saline $p = 0.1012$, MIA $p = 0.0280$) (Parvalbumin- MIA: $F_{(1,8)} = 30.45$, $p = 0.0006$; Cre: $F_{(1,8)} = 0.1830$, $p = 0.6801$; MIAxCre: $F_{(1,8)} = 5.403$, $p = 0.0486$; *Post hoc*- Saline v.s. MIA: *Cre*$^-$ $p = 0.0005$, *Cre*$^+$ $p = 0.0539$; *Cre*$^-$ v.s. *Cre*$^+$: Saline $p = 0.2167$, MIA $p = 0.0875$). All groups n = 3 l (1–2 offspring per group) (Two-way ANOVA with Fisher's LSD *post hoc* test). $^*p < 0.05$, $^{**}p < 0.01$, $^{***}p < 0.001$ between groups (Data are presented as mean ± SEM. ML: molecular layer, GCL: granule cell layer, PCL: Purkinje cell layer. n.s.: not significant.

and adult behavior. Our study demonstrates that placental IL-6 signaling, specifically in the trophoblast, is required for MIA-induced acute immune activation in the fetal brain, as well as downstream neuropathologies and behavioral impairments (see model diagram in Fig. 6). These findings contribute to the increasing appreciation that interactions at the maternal-placental-fetal interface play an important role in relaying the effects of maternal gestational insults to the developing embryo.

However, the events linking transiently elevated fetal brain cytokines to neuropathologies and behavioral deficits remain to be defined. Previous studies of the MIA model reveal that although MIA itself is transient, it results in dynamic and long-lasting changes to cytokine profiles across gross regions of the early postnatal and adult brain (Garay et al., 2013). In addition, MIA in mothers leads to durable programming of persistent immune dysregulation in adult offspring (Hsiao et al., 2012). Epigenetic alterations have been reported in MIA, and may mediate the long-term effects of transient immune activation (Connor et al., 2012). Therefore, transient induction of IL-6 in the fetal brain, during critical period of neurodevelopment, appear to set in motion events that lead to adverse neuropathological and behavioral outcomes in adulthood.

Herein, we demonstrate that initiating the MIA cascade through placental IL-6 signaling leads to adverse effects in the offspring. Three different pathways may contribute to the link between placental IL-6 expression and downstream responses in the fetal brain. First, the placenta may initiate a feed-forward cycle of IL-6 induction in the embryo. Maternal IL-6 can directly cross the placenta and reach the fetus during mid-gestation, but not late gestation in rats, which aligns well with the finding that the placenta exhibits higher permeability during mid-gestation compared to late gestation (Dahlgren et al., 2006). Interestingly, expression of suppressor of cytokine signaling 3 (SOCS3), a key factor involved in the negative inhibition of IL-6 activity, is absent in the SP layer of placenta between E7-E14, while both STAT3 and pSTAT3 are present (San Martin et al., 2013), which may support the notion that IL-6 triggers a feed-forward cycle of cytokine signaling to propagate the MIA inflammatory signal in the absence of its native suppressor.

A second potential mechanism underlying the link between placental IL-6 signaling and fetal brain status is modulation of placental hormones. Hormone imbalance could profoundly impact placental and embryonic development. We find herein that placental *Prl2b1* gene expression is upregulated after MIA, but absent in placenta lacking trophoblast-specific IL-6 signaling. *Prl2b1* is speculated to play a role in the regulation of placental angiogenesis and uterine growth (Dai et al., 2000). Further, placental corticotrophin-releasing factor (CRF) signaling is another pathway that may affect MIA response. Placenta derived CRF secretion has been shown in response to different conditions during pregnancy, including infectious stress (Florio et al., 2002). *In vitro* studies reveal that CRF can inhibit IL-6 production induced by endotoxin in human mononuclear cells (Hagan et al., 1992), which suggest other possible mechanisms for CRF activity in contributing to MIA dependent outcomes. Future studies warrant examination of additional placental hormones and functional evaluation of how changes in their expression impact embryonic development.

A third pathway by which placental IL-6Rα signaling may lead to altered neurodevelopment involves an effect of MIA directly on placental permeability. In the placenta, tight junction proteins provide a barrier between the mother and fetus in regulating the exchange of materials, and the permeability of the placenta can be altered during inflammation. Chorioamnionitis-induced upregulation of pro-inflammatory cytokines decreases expression of tight junction proteins in trophoblastic and endothelial cells of the placenta, facilitating infection (Tossetta et al., 2014). Furthermore, co-culture of human umbilical vein endothelial cells with the placental trophoblast cells from women with preeclampsia results in decreased barrier function of endothelial cells. The endothelial tight junctions become more vulnerable, which indicates that placenta trophoblast-derived factors are able to change the vascular permeability in the placenta (Wang et al., 2004). How such changes in the placenta alter the metabolic and nutrient milieu in the developing embryo is unclear. However, our previous study discovered that MIA offspring display increased gut permeability, which allows potentially neurotoxic molecules to leak into the circulation and impact behavior (Hsiao et al., 2013). Tracking metabolites from mother to fetus following placental IL-6 signaling may reveal insights into biological links between placental status and neurodevelopment.

Notably, the role of soluble IL-6Rα (sIL-6Rα) in the MIA model is still not clear. In mouse, 93.4% of circulating sIL-6Rα is contributed by granulocytes, macrophages, and hepatocytes as demonstrated by a conditional IL-6Rα knockout approach (McFarland-Mancini

Please cite this article in press as: Wu, W.-L., et al. The placental interleukin-6 signaling controls fetal brain development and behavior. Brain Behav. Immun. (2016), http://dx.doi.org/10.1016/j.bbi.2016.11.007

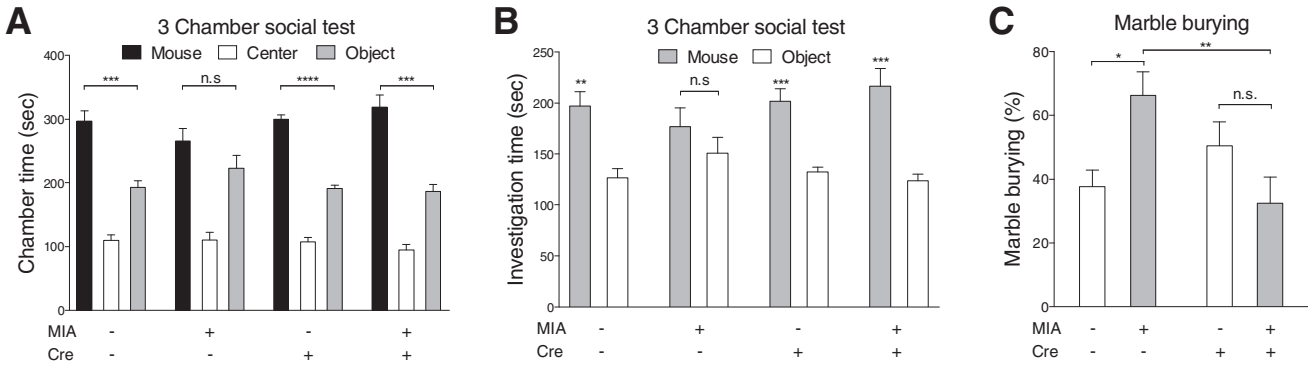

Fig. 5. Deletion of placental trophoblast *Il6ra* prevents behavioral abnormalities in MIA offspring. (A and B) Offspring social behavior was assessed by 3-chamber social test. Maternal saline treated offspring display social preference, whereas they spend more time in the mouse chamber over than object chamber. On the contrary, MIA *Il6ra*$^{fl/fl}$ offspring do not have social preference. Deletion of placental IL-6Rα in MIA offspring display social preference (A) Mouse v.s. Object: Student's two-tailed unpaired *t* test; Chamber duration: Saline *Cre*$^{-}$ t_{10} = 5.505, p = 0.0003, MIA *Cre*$^{-}$ t_{10} = 1.503, p = 0.1637, Saline *Cre*$^{+}$ t_{10} = 12.71, p < 0.0001, MIA *Cre*$^{+}$ t_{10} = 6.032, p = 0.0001. (B) Mouse v.s. Object: Student's two-tailed unpaired *t* test; Cup investigation time: Saline *Cre*$^{-}$ t_{10} = 4.195, p = 0.0018, MIA *Cre*$^{-}$ t_{10} = 1.081, p = 0.3053, Saline *Cre*$^{+}$ t_{10} = 5.1777, p = 0.0004, MIA *Cre*$^{+}$ t_{10} = 4.957, p = 0.0006. All groups n = 6 l (22, 22, 19, 25 offspring were used for Saline *Cre*$^{-}$; MIA *Cre*$^{-}$; Saline *Cre*$^{+}$; MIA *Cre*$^{+}$, respectively). (C) Stereotypic/repetitive behavior was measured by marble burying test. Increased repetitive marble burying behavior is seen in MIA *Il6ra*$^{fl/fl}$ offspring, but abrogated in MIA *Cyp19-Cre*$^{+}$;*Il6ra*$^{fl/fl}$ offspring (MIA: $F_{(1,20)}$ = 0.5537, p = 0.4655; Cre: $F_{(1,8)}$ = 2.156, p = 0.1576; MIAxCre: $F_{(1,8)}$ = 10.55, p = 0.0040; *Post hoc*- Saline v.s. MIA: *Cre*$^{-}$ p = 0.0105, *Cre*$^{+}$ p = 0.0919; *Cre*$^{-}$ v.s. *Cre*$^{+}$: Saline p = 0.2226, MIA p = 0.0033) (Two-way ANOVA with Fisher's LSD *post hoc* test). All groups n = 6 l (22, 22, 26, 25 offspring were used for Saline *Cre*$^{-}$; MIA *Cre*$^{-}$; Saline *Cre*$^{+}$; MIA *Cre*$^{+}$, respectively). $^{*}p < 0.05$, $^{**}p < 0.01$, $^{***}p < 0.001$, $^{****}p < 0.0001$ between groups. Data are presented as mean ± SEM. n.s.: not significant.

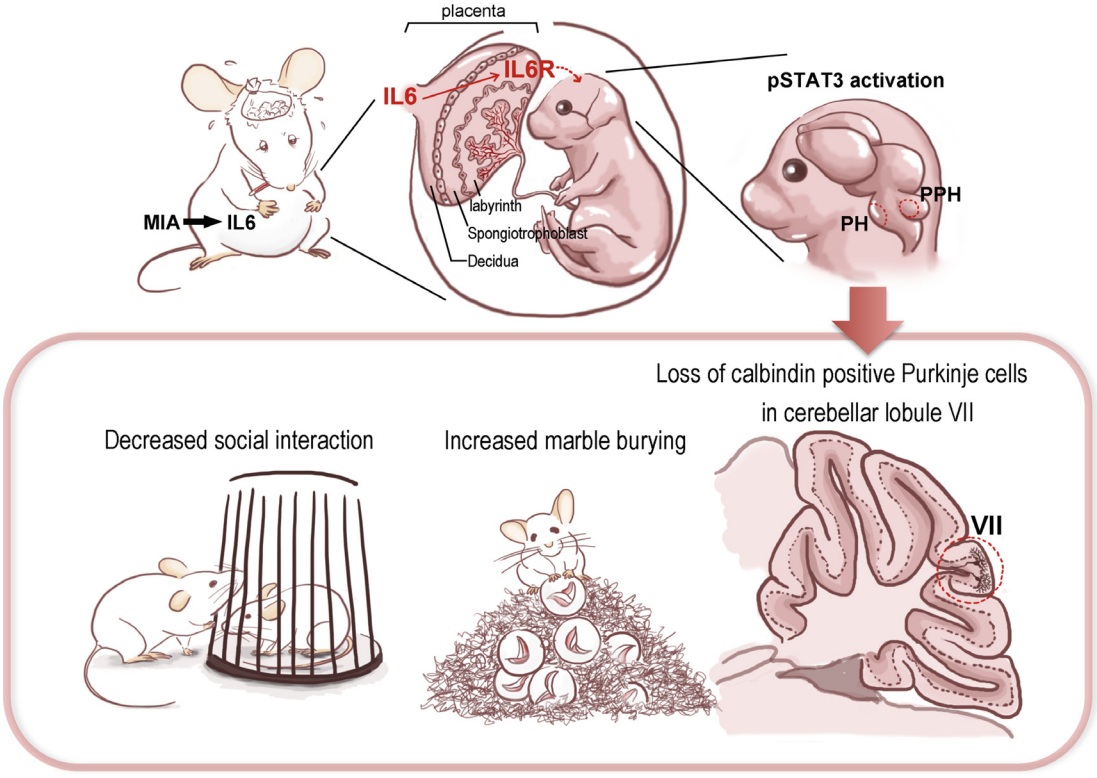

Fig. 6. A schematic model of how spongiotrophoblast IL-6Rα deletion prevents the behavioral abnormalities and cerebellum neuropathologies causing by MIA. PPH: prepontine hindbrain; PH: pontine hindbrain.

et al., 2010). *Cyp19-Cre* is expressed in trophoblast precursor cells and predominately distributed within the spongiotrophoblasts, labyrinth trophoblasts, and giant cells of the placenta (Wenzel and Leone, 2007). While the *Cyp19-Cre*$^{+}$;*Il6ra*$^{fl/fl}$ mice used in this study exhibited intended deficiencies in placental IL-6R gene expression, whether signaling through sIL-6Rα occurs on IL-6R-deficient trophoblasts is unclear. sIL-6Rα is thought to be derived by either proteolytic cleavage of the membrane moiety to liberate the extracellular portion of the receptor or by alternative splicing of the IL-6R transcript. It is possible that sIL-6Rα derived from non-trophoblastic sources in the placenta or from the maternal bloodstream could bind to gp130 on IL-6R-deficient trophoblasts; however, our data showing that MIA-associated STAT3 activation is abrogated in trophoblast cells from *Cyp19-Cre*$^{+}$;*Il6ra*$^{fl/fl}$ mice suggests that signaling through any available sIL-6Rα is not a major confounding factor. Additional studies are warranted to examine the role of sIL-6Rα in the MIA model.

Although we observe that blocking IL-6 signaling in MIA placenta successfully prevents detrimental effects to the offspring, whether direct infiltration of inflammatory cells into the placenta

Please cite this article in press as: Wu, W.-L., et al. The placental interleukin-6 signaling controls fetal brain development and behavior. Brain Behav. Immun. (2016), http://dx.doi.org/10.1016/j.bbi.2016.11.007

is involved in this MIA response remains unclear. We previously demonstrated MIA increased CD69 expression in decidual natural killer cells (uterine NK, uNK), macrophages and granulocytes (Hsiao and Patterson, 2011). The elevation of CD69 expression in leukocyte populations was unchanged when induced MIA in IL-6 deficient dam, indicating that placental inflammatory cell activation is independent of IL-6 action (Hsiao and Patterson, 2011). In preliminary studies, we observed no overt infiltration of uNK cells or myeloid cells from the decidua or maternal blood spaces into the placenta at 3, 6 or 24 h post MIA induction, but whether other subtypes of immune cells or other time points may be affected requires further study.

Our study demonstrates that blocking IL-6 signaling in the placenta prevents the development of a robust neuropathology in ASD, a spatially-restricted deficit in Purkinje cells in lobule VII of the cerebellum. Cerebellar injury at birth is a strong risk factor for ASD (Wang et al., 2014). Postmortem studies reveal Purkinje cell abnormalities in ASD patients (Skefos et al., 2014; Whitney et al., 2008). Most pSTAT3^{+} cells in the fetal brain of MIA offspring are located at cerebellum primordium of PPH. The cerebellum arises from the PPH, specifically rhombomere 1 at E9 of gestation, and develops into the wing-like cerebellar primordium by E12.5 in mice. Purkinje cells arise around E10–E13 (Hashimoto and Mikoshiba, 2003; Miale and Sidman, 1961). Postmitotic Purkinje cells undergo a migration process at E12.5-E15 and start to express calbindin at E14 (Sillitoe and Joyner, 2007; Wang and Zoghbi, 2001). MIA is induced during this critical window of Purkinje cell development at E12.5. In addition, the other region with elevated pSTAT3 is located at the trigeminal ganglion afferents area of PH. It has been demonstrated that by altering hindbrain transcription factors during embryonic stage, the nerve ascending from the trigeminal ganglion ectopically projects into the cerebellum instead of hindbrain (Oury et al., 2006). Based on these finding, hypothetically, induction of MIA in the fetus at E12.5 might directly disrupt cerebellum development, Purkinje cells generation and hindbrain neural circuitry formation. Blocking IL-6 signaling in the placenta during the acute phase of infection is capable of reducing STAT3 activation in the cerebellar primordium of the fetus, and also prevents the deficiency in Purkinje cells seen in the cerebellum of MIA offspring.

We hypothesize that the loss of Purkinje cells in lobule VII of the cerebellum in MIA adult offspring is due to an alterations in developmental trajectory. Previous studies revealed that deficiencies in lobule VII Purkinje cells could be observed as early as postnatal day 11 in offspring of mothers infected with influenza. Moreover, abnormal migration of Purkinje cells was also observed at this stage, with ectopic placement of some Purkinje cells within the cerebellar lobules (Shi et al., 2009). Based on these findings, we speculate that the loss of Purkinje cells observed in adult MIA offspring may result from a common mechanism as seen in the infection model, where the generalized maternal inflammatory response causes the loss of Purkinje cells in lobule VII in offspring during early development.

Traditionally, the cerebellum is regarded as the brain region responsible for controlling motor-related tasks. More recent evidence suggests that the cerebellum may be an essential component in processing external sensory inputs to govern movement and higher cognitive function (Wang et al., 2014). The association between ASD-like behaviors and the loss of cerebellar Purkinje cells has been reported in several mouse models with features of ASD-like behavior (Fujita et al., 2012; Reith et al., 2013; Tsai et al., 2012). Functional MRI studies demonstrate the connectivity of cerebellum lobule VII and the pre-prefrontal and posterior-parietal cortices, which implies lobule VII might be involved in higher cognitive function (Habas et al., 2009; O'Reilly et al., 2010). Disruption of cerebellar lobule VII development at the embryonic stage may produce cognitive impairment in offspring, which again points to the importance of intervention of immune activation in the maternal environment during the acute phase of infection.

The role of trigeminal afferent neurons and associated brain nuclei is relatively not well understood in ASD. Whether MIA disrupts hindbrain pattern formation and development of trigeminal system via activation of inflammatory signaling in the PH, a brain region that receives inputs from the trigeminal ganglion, will need further investigation. Prenatal exposure of valproic acid (VPA) is another model of an environmental risk factor for autism. Intriguingly, injection of VPA between E11.5 and 12.5 leads to reduction of motor neuron number in the trigeminal motor nucleus in rat pups (Rodier et al., 1996). Furthermore, VPA injection decreases immunoreactivity of neurofilaments in the trigeminal nerves of the embryo (Tashiro et al., 2011). Collectively, these studies suggest a possible mechanism by which MIA and other maternal insults could perturb development of trigeminal innervations.

As IL-6 is a pro-inflammatory cytokine in response to bacterial and viral infections, the prophylactic effect of blocking IL-6 signaling in placenta could widely applicable across different modes of maternal infection. We hypothesize that this preventive effect is not only limited to maternal toll-like receptor 3 (TLR3) activation, as we demonstrate by using poly(I:C), but can also be effective for other types of maternal immune activation, e.g. prenatal activation of TLR4 by administration of the bacterial endotoxin lipopolysaccharide (LPS). Prenatal challenge with LPS similarly increases placental IL-6 during the acute phase of infection in both *in vivo* and *in vitro* models (Anton et al., 2012; Bell et al., 2004; Bloise et al., 2013; Jin et al., 2015; Urakubo et al., 2001). Furthermore, histopathology approaches indicate that prenatal administration of LPS causes mesenchymal hyperplasia, infiltration of neutrophils in the placental labyrinth and increase of fibrin deposition at both the spongiotrophoblast and labyrinth zone (Jin et al., 2015). Moreover, maternal LPS challenge has also been shown to activate pSTAT3 in the fetal brain. This pSTAT3 activation in the fetal brain can be neutralized by IL-6 antibody (Mouihate and Mehdawi, 2016), indicating IL-6/STAT3 signaling is the key pathway for prenatal LPS administration. These results lead to a converging mechanism by which maternal infection impacts placental and fetal development via placental IL-6 signaling. Our findings support a causal role for placental IL-6/IL-6Rα/STAT3 in MIA models.

In conclusion, our study reveals that MIA induces an IL-6 surge in the maternal-placental-fetal axis, resulting in acute fetal brain responses and long-term changes in brain development and behavior. We identify signaling of placentally-derived IL-6 through IL-6Rα on placenta trophoblasts as a key step for relaying the MIA response from mother to fetus. Blocking IL-6 signaling in the placenta by trophoblast-specific deletion of IL-6Rα effectively prevents downstream immune responses in the fetal brain and precludes the development of Purkinje cell deficits and ASD-related behaviors in adult offspring. These data contribute to the increasing appreciation for the important role of maternal-fetal interactions at the placenta in guiding embryonic neurodevelopment. Moreover, our findings suggest that blocking placental IL-6 signaling during the acute phase of infection can serve as a preventative therapeutic for the development of neuropathological and behavioral symptoms of ASD in at-risk populations.

Financial disclosures

All authors declare no conflicts of interest related to this work.

Acknowledgments

We acknowledge Drs. H. Chu, A. Khoshnan, B.D. Needham, T.R. Sampson, C.E. Schretter, and G. Sharon for critically reviewing the

Please cite this article in press as: Wu, W.-L., et al. The placental interleukin-6 signaling controls fetal brain development and behavior. Brain Behav. Immun. (2016), http://dx.doi.org/10.1016/j.bbi.2016.11.007

manuscript; Professor G. Leone for providing the *Cyp19-Cre* mouse line; Professor D.J. Anderson for providing *ROSA::LSL-lacZ* mice; Professor A.J. Varshavsky for providing *Ate1*$^{-/-}$ *mouse*; Professor J.M. Allman for use of the LCM equipment; Professor B.J. Wold for use of a cryostat; Dr. B. Williams for training and use of LCM and cryostat equipment; Dr. A. Collazo and Caltech Biological Imaging Center for the training and use of confocal microscope; L. Rodriguez for administrative assistance; J. Gutierrez, K.F. Lee, J. Rodriguez, L.C. Sandoval, N.A. Verduzco for caring of animals. This work was supported by NIH Conte Center Award, United States (NIH 5P50MH086383-04, to P.H.P.); Autism Speaks (#7670, to P.H.P); Postdoctoral Fellowship from National Science Council, Taiwan (NSC 101-2917-I-564-039, to W.-L.W.); Autism Speaks Weatherstone Predoctoral Fellowship (to E.Y.H.) and NIH/NRSA Predoctoral Fellowship, United States (to E.Y.H.); Caltech Undergraduate Research Fellowship (SURF) (to Z.Y.) and Amgen Scholars Program at Caltech (to Z.Y.); the Heritage Medical Research Institute (to S.K.M.), Simons Foundation (to S.K.M.), and NIH, United States (MH100556 to S.K.M.).

Appendix A. Supplementary data

Supplementary data associated with this article can be found, in the online version, at http://dx.doi.org/10.1016/j.bbi.2016.11.007.

References

Anderson, G.M., Jacobs-Stannard, A., Chawarska, K., Volkmar, F.R., Kliman, H.J., 2007. Placental trophoblast inclusions in autism spectrum disorder. Biol. Psychiatry 61, 487–491.

Anton, L., Brown, A.G., Parry, S., Elovitz, M.A., 2012. Lipopolysaccharide induces cytokine production and decreases extravillous trophoblast invasion through a mitogen-activated protein kinase-mediated pathway: possible mechanisms of first trimester placental dysfunction. Hum. Reprod. 27, 61–72.

Ashwood, P., Krakowiak, P., Hertz-Picciotto, I., Hansen, R., Pessah, I., Van de Water, J., 2011. Elevated plasma cytokines in autism spectrum disorders provide evidence of immune dysfunction and are associated with impaired behavioral outcome. Brain Behav. Immun. 25, 40–45.

Association, A.P., 2013. Diagnostic and Statistical Manual of Mental Disorders: Dsm-5. American Psychiatric Association, Washington, D.C..

Atladottir, H.O., Thorsen, P., Ostergaard, L., Schendel, D.E., Lemcke, S., Abdallah, M., Parner, E.T., 2010. Maternal infection requiring hospitalization during pregnancy and autism spectrum disorders. J. Autism Dev. Disord. 40, 1423–1430.

Bell, M.J., Hallenbeck, J.M., Gallo, V., 2004. Determining the fetal inflammatory response in an experimental model of intrauterine inflammation in rats. Pediatr. Res. 56, 541–546.

Bloise, E., Bhuiyan, M., Audette, M.C., Petropoulos, S., Javam, M., Gibb, W., Matthews, S.G., 2013. Prenatal endotoxemia and placental drug transport in the mouse: placental size-specific effects. PLoS ONE 8, e65728.

Boksa, P., 2010. Effects of prenatal infection on brain development and behavior: a review of findings from animal models. Brain Behav. Immun. 24, 881–897.

Brower, C.S., Varshavsky, A., 2009. Ablation of arginylation in the mouse N-end rule pathway: loss of fat, higher metabolic rate, damaged spermatogenesis, and neurological perturbations. PLoS ONE 4, e7757.

Brown, A.S., 2012. Epidemiologic studies of exposure to prenatal infection and risk of schizophrenia and autism. Dev. Neurobiol. 72, 1272–1276.

Chow, K.H., Yan, Z., Wu, W.L., 2016. Induction of maternal immune activation in mice at mid-gestation stage with viral mimic Poly(I:C). J. Visualized Exp. JoVE.

Coghlan, S., Horder, J., Inkster, B., Mendez, M.A., Murphy, D.G., Nutt, D.J., 2012. GABA system dysfunction in autism and related disorders: from synapse to symptoms. Neurosci. Biobehav. Rev. 36, 2044–2055.

Connor, C.M., Dincer, A., Straubhaar, J., Galler, J.R., Houston, I.B., Akbarian, S., 2012. Maternal immune activation alters behavior in adult offspring, with subtle changes in the cortical transcriptome and epigenome. Schizophr. Res. 140, 175–184.

Courchesne, E., 1997. Brainstem, cerebellar and limbic neuroanatomical abnormalities in autism. Curr. Opin. Neurobiol. 7, 269–278.

Dahlgren, J., Samuelsson, A.M., Jansson, T., Holmang, A., 2006. Interleukin-6 in the maternal circulation reaches the rat fetus in mid-gestation. Pediatr. Res. 60, 147–151.

Dai, G., Wang, D., Liu, B., Kasik, J.W., Muller, H., White, R.A., Hummel, G.S., Soares, M. J., 2000. Three novel paralogs of the rodent prolactin gene family. J. Endocrinol. 166, 63–75.

Davis, J.O., Phelps, J.A., Bracha, H.S., 1995. Prenatal development of monozygotic twins and concordance for schizophrenia. Schizophr. Bull. 21, 357–366.

Elsabbagh, M., Divan, G., Koh, Y.J., Kim, Y.S., Kauchali, S., Marcin, C., Montiel-Nava, C., Patel, V., Paula, C.S., Wang, C., Yasamy, M.T., Fombonne, E., 2012. Global prevalence of autism and other pervasive developmental disorders. Autism Res. 5, 160–179.

Fatemi, S.H., Folsom, T.D., Rooney, R.J., Mori, S., Kornfield, T.E., Reutiman, T.J., Kneeland, R.E., Liesch, S.B., Hua, K., Hsu, J., Patel, D.H., 2012. The viral theory of schizophrenia revisited: abnormal placental gene expression and structural changes with lack of evidence for H1N1 viral presence in placentae of infected mice or brains of exposed offspring. Neuropharmacology 62, 1290–1298.

Florio, P., Severi, F.M., Ciarmela, P., Fiore, G., Calonaci, G., Merola, A., De Felice, C., Palumbo, M., Petraglia, F., 2002. Placental stress factors and maternal-fetal adaptive response: the corticotropin-releasing factor family. Endocrine 19, 91–102.

Fujita, E., Tanabe, Y., Momoi, M.Y., Momoi, T., 2012. Cntnap2 expression in the cerebellum of Foxp 2(R552H) mice, with a mutation related to speech-language disorder. Neurosci. Lett. 506, 277–280.

Furbass, R., Selimyan, R., Vanselow, J., 2008. DNA methylation and chromatin accessibility of the proximal Cyp 19 promoter region 1.5/2 correlate with expression levels in sheep placentomes. Mol. Reprod. Dev. 75, 1–7.

Garay, P.A., Hsiao, E.Y., Patterson, P.H., McAllister, A.K., 2013. Maternal immune activation causes age- and region-specific changes in brain cytokines in offspring throughout development. Brain Behav. Immun. 31, 54–68.

Habas, C., Kamdar, N., Nguyen, D., Prater, K., Beckmann, C.F., Menon, V., Greicius, M. D., 2009. Distinct cerebellar contributions to intrinsic connectivity networks. J. Neurosci. 29, 8586–8594.

Hagan, P., Poole, S., Bristow, A.F., 1992. Immunosuppressive activity of corticotrophin-releasing factor. Inhibition of interleukin-1 and interleukin-6 production by human mononuclear cells. Biochem. J. 281 (Pt 1), 251–254.

Hashimoto, M., Mikoshiba, K., 2003. Mediolateral compartmentalization of the cerebellum is determined on the "birth date" of Purkinje cells. J. Neurosci. 23, 11342–11351.

Hsiao, E.Y., Patterson, P.H., 2011. Activation of the maternal immune system induces endocrine changes in the placenta via IL-6. Brain Behav. Immun. 25, 604–615.

Hsiao, E.Y., McBride, S.W., Chow, J., Mazmanian, S.K., Patterson, P.H., 2012. Modeling an autism risk factor in mice leads to permanent immune dysregulation. Proc. Natl. Acad. Sci. U.S.A. 109, 12776–12781.

Hsiao, E.Y., McBride, S.W., Hsien, S., Sharon, G., Hyde, E.R., McCue, T., Codelli, J.A., Chow, J., Reisman, S.E., Petrosino, J.F., Patterson, P.H., Mazmanian, S.K., 2013. Microbiota modulate behavioral and physiological abnormalities associated with neurodevelopmental disorders. Cell 155, 1451–1463.

Investigators, A.a.D.D.M.N.S.Y.P., 2014. Prevalence of Autism Spectrum Disorder Among Children Aged 8 Years — Autism and Developmental Disabilities Monitoring Network, 11 Sites, United States, 2010. In: Prevention, C.f.D.C.a. (Ed.), Surveillance Summaries, pp. 1–21.

Jin, S.J., Liu, Y., Deng, S.H., Liao, L.H., Lin, T.L., Ning, Q., Luo, X.P., 2015. Neuroprotective effects of activated protein C on intrauterine inflammation-induced neonatal white matter injury are associated with the downregulation of fibrinogen-like protein 2/fibroleukin prothrombinase and the inhibition of pro-inflammatory cytokine expression. Int. J. Mol. Med. 35, 1199–1212.

Knuesel, I., Chicha, L., Britschgi, M., Schobel, S.A., Bodmer, M., Hellings, J.A., Toovey, S., Prinssen, E.P., 2014. Maternal immune activation and abnormal brain development across CNS disorders. Nat. Rev. Neurol. 10, 643–660.

Lee, B.K., Magnusson, C., Gardner, R.M., Blomstrom, S., Newschaffer, C.J., Burstyn, I., Karlsson, H., Dalman, C., 2014. Maternal hospitalization with infection during pregnancy and risk of autism spectrum disorders. Brain Behav. Immun.

Li, X., Chauhan, A., Sheikh, A.M., Patil, S., Chauhan, V., Li, X.M., Ji, L., Brown, T., Malik, M., 2009. Elevated immune response in the brain of autistic patients. J. Neuroimmunol. 207, 111–116.

Malkova, N.V., Yu, C.Z., Hsiao, E.Y., Moore, M.J., Patterson, P.H., 2012. Maternal immune activation yields offspring displaying mouse versions of the three core symptoms of autism. Brain Behav. Immun. 26, 607–616.

Masi, A., Quintana, D.S., Glozier, N., Lloyd, A.R., Hickie, I.B., Guastella, A.J., 2014. Cytokine aberrations in autism spectrum disorder: a systematic review and meta-analysis. Mol. Psychiatry.

McFarland-Mancini, M.M., Funk, H.M., Paluch, A.M., Zhou, M., Giridhar, P.V., Mercer, C.A., Kozma, S.C., Drew, A.F., 2010. Differences in wound healing in mice with deficiency of IL-6 versus IL-6 receptor. J. Immunol. 184, 7219–7228.

Meyer, U., 2014. Prenatal poly(i:C) exposure and other developmental immune activation models in rodent systems. Biol. Psychiatry 75, 307–315.

Meyer, U., Nyffeler, M., Engler, A., Urwyler, A., Schedlowski, M., Knuesel, I., Yee, B.K., Feldon, J., 2006. The time of prenatal immune challenge determines the specificity of inflammation-mediated brain and behavioral pathology. J. Neurosci. 26, 4752–4762.

Miale, I.L., Sidman, R.L., 1961. An autoradiographic analysis of histogenesis in the mouse cerebellum. Exp. Neurol. 4, 277–296.

Mouihate, A., Mehdawi, H., 2016. Toll-like receptor 4-mediated immune stress in pregnant rats activates STAT3 in the fetal brain: role of interleukin-6. Pediatr. Res. 79, 781–787.

Naviaux, R.K., Zolkipli, Z., Wang, L., Nakayama, T., Naviaux, J.C., Le, T.P., Schuchbauer, M.A., Rogac, M., Tang, Q., Dugan, L.L., Powell, S.B., 2013. Antipurinergic therapy corrects the autism-like features in the poly(IC) mouse model. PLoS ONE 8, e57380.

O'Reilly, J.X., Beckmann, C.F., Tomassini, V., Ramnani, N., Johansen-Berg, H., 2010. Distinct and overlapping functional zones in the cerebellum defined by resting state functional connectivity. Cereb. Cortex 20, 953–965.

Oury, F., Murakami, Y., Renaud, J.S., Pasqualetti, M., Charnay, P., Ren, S.Y., Rijli, F.M., 2006. Hoxa2- and rhombomere-dependent development of the mouse facial somatosensory map. Science 313, 1408–1413.

Puelles, L., Harrison, M., Paxinos, G., Watson, C., 2013. A developmental ontology for the mammalian brain based on the prosomeric model. Trends Neurosci. 36, 570–578.

Rawn, S.M., Cross, J.C., 2008. The evolution, regulation, and function of placenta-specific genes. Annu. Rev. Cell Dev. Biol. 24, 159–181.

Reith, R.M., McKenna, J., Wu, H., Hashmi, S.S., Cho, S.H., Dash, P.K., Gambello, M.J., 2013. Loss of Tsc2 in Purkinje cells is associated with autistic-like behavior in a mouse model of tuberous sclerosis complex. Neurobiol. Dis. 51, 93–103.

Rodier, P.M., Ingram, J.L., Tisdale, B., Nelson, S., Romano, J., 1996. Embryological origin for autism: developmental anomalies of the cranial nerve motor nuclei. J. Comp. Neurol. 370, 247–261.

Ronald, A., Hoekstra, R.A., 2011. Autism spectrum disorders and autistic traits: a decade of new twin studies. Am. J. Med. Gen. Part B, Neuropsychiatr. Gen. 156B, 255–274.

San Martin, S., Fitzgerald, J.S., Weber, M., Parraga, M., Saez, T., Zorn, T.M., Markert, U. R., 2013. Stat3 and Socs3 expression patterns during murine placenta development. Eur. J. Histochem. EJH 57, e19.

Shi, L., Tu, N., Patterson, P.H., 2005. Maternal influenza infection is likely to alter fetal brain development indirectly: the virus is not detected in the fetus. Int. J. Dev. Neurosci. 23, 299–305.

Shi, L., Smith, S.E., Malkova, N., Tse, D., Su, Y., Patterson, P.H., 2009. Activation of the maternal immune system alters cerebellar development in the offspring. Brain Behav. Immun. 23, 116–123.

Sillitoe, R.V., Joyner, A.L., 2007. Morphology, molecular codes, and circuitry produce the three-dimensional complexity of the cerebellum. Annu. Rev. Cell Dev. Biol. 23, 549–577.

Skefos, J., Cummings, C., Enzer, K., Holiday, J., Weed, K., Levy, E., Yuce, T., Kemper, T., Bauman, M., 2014. Regional alterations in purkinje cell density in patients with autism. PLoS ONE 9, e81255.

Smith, S.E., Li, J., Garbett, K., Mirnics, K., Patterson, P.H., 2007. Maternal immune activation alters fetal brain development through interleukin-6. J. Neurosci. 27, 10695–10702.

Spandidos, A., Wang, X., Wang, H., Seed, B., 2010. PrimerBank: a resource of human and mouse PCR primer pairs for gene expression detection and quantification. Nucleic Acids Res. 38, D792–D799.

Tashiro, Y., Oyabu, A., Imura, Y., Uchida, A., Narita, N., Narita, M., 2011. Morphological abnormalities of embryonic cranial nerves after in utero exposure to valproic acid: implications for the pathogenesis of autism with multiple developmental anomalies. Int. J. Dev. Neurosci. 29, 359–364.

Tossetta, G., Paolinelli, F., Avellini, C., Salvolini, E., Ciarmela, P., Lorenzi, T., Emanuelli, M., Toti, P., Giuliante, R., Gesuita, R., Crescimanno, C., Voltolini, C., Di Primio, R., Petraglia, F., Castellucci, M., Marzioni, D., 2014. IL-1beta and TGF-beta weaken the placental barrier through destruction of tight junctions: an in vivo and in vitro study. Placenta 35, 509–516.

Tsai, P.T., Hull, C., Chu, Y., Greene-Colozzi, E., Sadowski, A.R., Leech, J.M., Steinberg, J., Crawley, J.N., Regehr, W.G., Sahin, M., 2012. Autistic-like behaviour and cerebellar dysfunction in Purkinje cell Tsc1 mutant mice. Nature 488, 647–651.

Urakubo, A., Jarskog, L.F., Lieberman, J.A., Gilmore, J.H., 2001. Prenatal exposure to maternal infection alters cytokine expression in the placenta, amniotic fluid, and fetal brain. Schizophr. Res. 47, 27–36.

Vargas, D.L., Nascimbene, C., Krishnan, C., Zimmerman, A.W., Pardo, C.A., 2005. Neuroglial activation and neuroinflammation in the brain of patients with autism. Ann. Neurol. 57, 67–81.

Walker, C.K., Anderson, K.W., Milano, K.M., Ye, S., Tancredi, D.J., Pessah, I.N., Hertz-Picciotto, I., Kliman, H.J., 2013. Trophoblast inclusions are significantly increased in the placentas of children in families at risk for autism. Biol. Psychiatry 74, 204–211.

Wang, V.Y., Zoghbi, H.Y., 2001. Genetic regulation of cerebellar development. Nat. Rev. Neurosci. 2, 484–491.

Wang, Y., Lewis, D.F., Gu, Y., Zhang, Y., Alexander, J.S., Granger, D.N., 2004. Placental trophoblast-derived factors diminish endothelial barrier function. J. Clin. Endocrinol. Metab. 89, 2421–2428.

Wang, S.S., Kloth, A.D., Badura, A., 2014. The cerebellum, sensitive periods, and autism. Neuron 83, 518–532.

Wei, H., Zou, H., Sheikh, A.M., Malik, M., Dobkin, C., Brown, W.T., Li, X., 2011. IL-6 is increased in the cerebellum of autistic brain and alters neural cell adhesion, migration and synaptic formation. J. Neuroinflammation 8, 52.

Wenzel, P.L., Leone, G., 2007. Expression of Cre recombinase in early diploid trophoblast cells of the mouse placenta. Genesis 45, 129–134.

Whitney, E.R., Kemper, T.L., Bauman, M.L., Rosene, D.L., Blatt, G.J., 2008. Cerebellar Purkinje cells are reduced in a subpopulation of autistic brains: a stereological experiment using calbindin-D28k. Cerebellum 7, 406–416.

Wu, W.L., Adams, C.E., Stevens, K.E., chow, K.H., Freedman, R., Patterson, P.H., 2015. The interaction between maternal immune activation and alpha 7 nicotinic acetylcholine receptor in regulating behaviors in the offspring. Brain Behav. Immun.

Yang, M., Silverman, J.L., Crawley, J.N., (2011). Automated three-chambered social approach task for mice. Current protocols in neuroscience/editorial board, Jacqueline N. Crawley Ellipsis et al., Unit 8 26.

Zaretsky, M.V., Alexander, J.M., Byrd, W., Bawdon, R.E., 2004. Transfer of inflammatory cytokines across the placenta. Obstet. Gynecol. 103, 546–550.

Ziats, M.N., Rennert, O.M., 2011. Expression profiling of autism candidate genes during human brain development implicates central immune signaling pathways. PLoS ONE 6, e24691.

Please cite this article in press as: Wu, W.-L., et al. The placental interleukin-6 signaling controls fetal brain development and behavior. Brain Behav. Immun. (2016), http://dx.doi.org/10.1016/j.bbi.2016.11.007